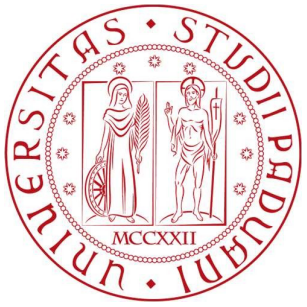

UNIVERSITÀ DEGLI STUDI DI PADOVA

SCUOLA DI SCIENZE

DIPARTIMENTO DI GEOSCIENZE

Direttore Prof. Nicola Surian

TESI DI LAUREA MAGISTRALE IN GEOLOGIA AMBIENTALE E DINAMICA DELLA TERRA

CHARACTERIZATION OF SOILS STABILIZED WITH SUSTAINABLE BINDERS

Relatore: Prof. Luca Valentini

Laureando: Sandra Mujombi

ANNO ACCADEMICO 2022/2023

ABSTRACT

Soils may have undesirable engineering properties because of their ability to adsorb large quantities of water and tendency to swell, therefore treating them to improve such properties becomes necessary when planning the construction of roads or other infrastructures. Due to seasonal moisture fluctuations, fine-grained soils enriched in clays and silts can suffer from serious problems such as loss of strength, compressibility, and swelling. This could result in adverse effects such as potholes and infrastructure failures, hence the need to stabilize the soils. Soil stabilization is the process of improving the shear strength parameters of a soil and thus increasing its bearing capacity in construction. It is common practice to use a variety of soil stabilization procedures to enhance engineering qualities and reduce moisture-induced volumetric changes in expansive soils.

Ordinary Portland cement (OPC) and lime are commonly used stabilizers, and their stabilization mechanisms are relatively well understood. The major issue with the production of conventional soil stabilizers (such as OPC and lime) is that they are energy intensive, deplete raw materials due to excessive demands and produce significant amounts of CO_2 emissions. For instance, approximately one ton of CO_2 is emitted for the production of one ton of cement. New low CO_2 binders are therefore needed to meet the global CO_2 reduction goals. Limestone calcined clay cement (LC^3) is a new type of cement that is made from a blend of 50% OPC clinker, limestone and calcined clay. LC^3 can reduce CO_2 emissions by up to 40%. It is made from limestone and low-grade clays which are abundant, is cost effective, and does not necessitate capital-intensive modifications to existing cement plants which makes it an excellent substitute for OPC. The objective of this research is to attempt to stabilize soils with more sustainable materials such as LC^3, hence providing a sustainable alternative whilst maintaining the required engineering properties of stabilized soils. The research work thus exemplifies the performance of the soil-LC^3 stabilized mixtures for their suitability in construction applications.

ACKNOWLEDGEMENT

This thesis was carried out within the framework of the Erasmus+ KA107 2020-2023 agreement between the University of Padua and the Meru University of Science and Technology. I would like to express my sincere gratitude to my supervisor, Professor Luca Valentini, for his invaluable guidance and support throughout my master's program. His expertise, helpful feedback and suggestions helped me to complete this research and write this thesis. I would also like to thank my colleagues at Meru University of Science and Technology, Dr. Joseph Mwiti Marangu and Muchui Loyford Mugambi for their support and collaboration during my research. I gratefully acknowledge the funding received towards my master's program from the Italian Ministry of Foreign Affairs and International Cooperation (MAECI). I would also like to say a heartfelt thank you to my family and friends for always believing in me and encouraging me to follow my dreams. Finally, I would like to extend my sincere gratitude to my husband, Goodluck Benjamin, who has been by my side throughout this master's program, living every single minute of it, and without whom, I would not have had the courage to embark on this journey in the first place.

Table of Contents

CHAPTER 1 - INTRODUCTION

1.1 Introduction to Soil Stabilization

This chapter presents an overview of current soil stabilization techniques and their sustainable alternatives, providing motivation to employ environmentally sustainable soil stabilization agents that are consistent with sustainability goals.

1.2 Aim

To reduce the environmental effects caused by the extensive use of Portland cement (OPC), researchers have sought various alternatives that would partially or completely replace it and one such alternative is "Limestone Calcined Clay Cement" (LC^3). Samples for this study were obtained from the Meru University of Science and Technology, Kenya where a preliminary study on the physicochemical properties was carried out by the local research team. The preliminary tests conducted on the samples were the Proctor test, California Bearing Ratio, Atterberg limits and compressive strength tests. From the results, LC^3 was deemed to be a suitable alternative to OPC at a dosage of 5% as it performed well for all the tests that were conducted. This study focuses on determining whether LC^3 is a viable alternative to OPC in soil stabilization at a microstructural scale. It examines soil stabilization using various materials including quarry dust, LC^3 and OPC. Several tests including calorimetry and volume stability were conducted to reveal the viability of each stabilization material in the relation of prime engineering properties such as swelling behavior, mechanical characteristics, and hydraulic parameters at the microstructural scale. To examine the observed behavior, mineralogical and microstructural tests such as Scanning Electron Microscopy (SEM) and X-Ray Diffraction (XRD) were also performed.

1.3 Soil Stabilization

Natural soil is a complex and variable material. When soil is exposed to water, it may shrink or swell due to the presence of clay minerals. Expansive soils are abundant throughout the world; however, they are regarded as problematic soils due to their moisture-sensitive nature, which results in adverse volumetric change behavior. Upon climatic variations, these soils exhibit swell-shrinkage behavior which could cause serious distress or failure to the overlying structures (Nauman I et al. 2022). During an earthquake, the contacts of expansive soil particles break down and become loose which leads to soil shear failure. Settlement of foundations, bulging, subsidence of roadways, and cracking in buildings and pavements are the types of structural failures associated with expansive soils that have been repeatedly discussed in the literature (Nauman I et al. 2022). Globally, expansive soils have cost billions of dollars in infrastructure damage. Given the magnitude of this problem, it is crucial to identify long-term solutions to mitigate its negative

effects in civil engineering projects to meet engineering specifications, hence the need for soil stabilization.

Soil stabilization refers to chemical or physical treatments that strengthen or maintain a soil's stability or improve its engineering qualities. The technique of soil stabilization has been adopted with the purpose of rendering plastic soils compliant with the standards and requirements of engineering projects. The principal benefits of soil stabilization are:

- Improving the workability of soils and their ability to be used in construction.
- Increasing the soil's bearing capacity.
- Reducing the soil's plasticity and shrink/swell volume change.
- Using onsite soil hence reducing the costs associated with removal and replacement.

1.4 Stabilization Agents

Different soil stabilization techniques are often adopted to improve engineering properties and to minimize moisture induced volumetric changes in expansive soils. Traditionally calcium-based stabilizers such as cement and lime have been used to stabilize soils because calcium saturated clay minerals have a reduced affinity for water and form cementitious products that resist volumetric changes, making them effective in controlling volume changes.

Ordinary Portland Cement (OPC) is extensively utilized for such soils due to its simplicity of access and practical understanding of mechanisms based on existing research (Barman and Dash, 2022; Chenarboni et al. 2021). The stabilization mechanisms in cement-stabilized soils are associated with hydration and pozzolanic reactions. Soil is stabilized through flocculation and pozzolanic reactions when cement or lime is mixed with clayey soils (Adaska WS. et al 2004). The extensive utilization of OPC in various construction sectors not only depletes natural resources but also has a significant environmental impact in terms of carbon emissions. Studies show that cement manufacturing is directly responsible for approximately 8% of artificial CO_2 emissions, with 0.8–1.1 tons of CO_2 released against each ton of cement production (Obrist et al. 2021). Furthermore, with the inexorable increase in urbanization and industrialization, cement consumption increases annually, which highlights the significance of recycling current approaches into greener alternatives that prioritize sustainability. Hence, alternative cementitious materials are required at this time in order to reduce the environmental strain caused by OPC while maintaining the serviceability required for construction applications.

To produce sustainable cement, it is of paramount importance to look at materials that are abundantly available in the earth's crust (primary resources) or technosphere (secondary resources). The use of Limestone Calcined Clay Cement (LC^3) as a partial replacement for clinker

in cement production has attracted a lot of attention because of the abundance of its components. The main ingredients in LC^3 are clinkers (50%), calcined clay (30%), limestone powder (15%), and gypsum (5%) which partially replace the clinker by 50% in comparison to conventional cement e.g., OPC (Scrivener et al. 2018). LC^3 has recently garnered considerable interest due to its low carbon footprint (about 30-40% less CO_2 emissions than traditional cement production) and lower cementitious material cost.

Solid waste material such as quarry dust can also be used for soil stabilization. Quarry dust is the by-product of extraction and processing of aggregates. Quarry dust is a hazardous waste that harms the environment and human health. It can be blended with other construction materials like clay and used best for various construction purposes to eliminate its negative effect and ensure viable disposal. Quarry dust exhibits high shear strength which is highly beneficial for its use as a geotechnical material (Sridharan A et al. 2006). It has good permeability, and variations in its water content have little impact on its properties. The shear strength of soil-quarry dust mixtures was investigated by (Sridharan et al. 2006). According to the findings, quarry dust is a promising alternative for sand that can be utilized to improve the engineering properties of soils and its addition increases the soil's dry density while decreasing the optimum moisture content.

1.5 Modification Mechanisms of Soil Stabilizers

The improved engineering properties in soil stabilization are achieved through four processes: cation exchange, flocculation, cement hydration and pozzolanic reactions.

Cation exchange

High plasticity in soils is mainly caused by the presence of Montmorillonite (an expansive clay). Its crystal structure is formed by the stacking of aluminum and silicate layers. As a result of montmorillonite's charge deficiency in its crystal structure, cations can enter the interlayer to neutralize the negative charge. When the neutralizing cation is monovalent, such as sodium, the clay becomes plastic. To minimize the plasticity of the clay, the monovalent cations present in the interlayer must be exchanged, which would result in a reduction in the thickness of the double layer, this occurs within hours. A good soil stabilizer should provide adequate calcium ions (Ca^{2+}) to replace the monovalent cations, particularly Na^{+}, in the interlayer.

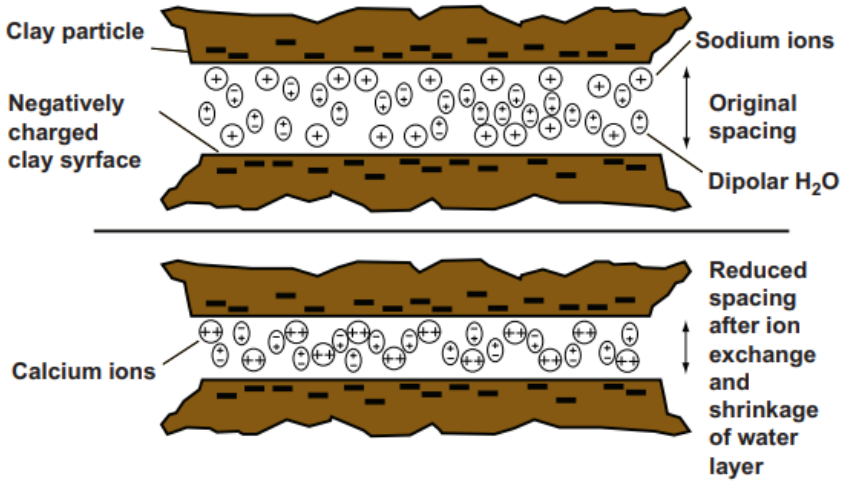

Figure 1: Cation exchange (Halsted et al. 2008)

Flocculation and cement hydration

As a result of the addition of cement, the soil is restructured. The process by which clay particles change their arrangement from a flat, parallel structure to a more random edge-to-face orientation is known as flocculation. Agglomeration is the weak bonding of clay particles at their edge-surface contacts. Soil particle restructuring due to flocculation and agglomeration transforms the texture from a plastic fine-grained material to a more granular soil. The reduced specific surface area as a result of flocculation and agglomeration, lead to lower plasticity, higher shear strength, and improved texture (Halsted et al. 2008). This phenomenon is shown in Fig. 2.

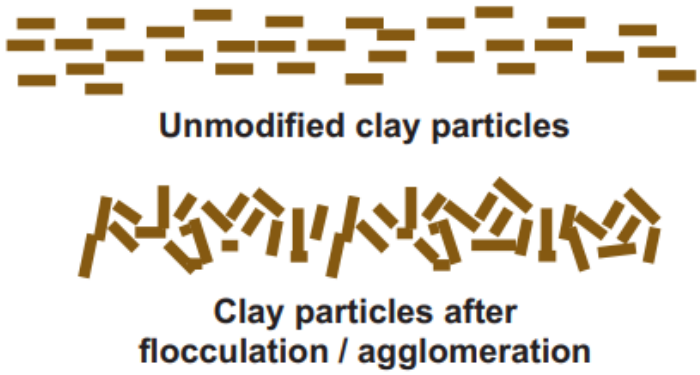

Figure 2: Particle restructuring (Halsted et al. 2008)

Cement hydration produces products such as calcium silicate hydrate (C-S-H) and calcium aluminum hydrate (C-A-H) which act as a binder. This binder adds structure to cement-modified soils by stabilizing the flocculated clay particles via clay-cement bonds. A high percentage of this reaction occurs within the first 30 days of adding cement to the soil.

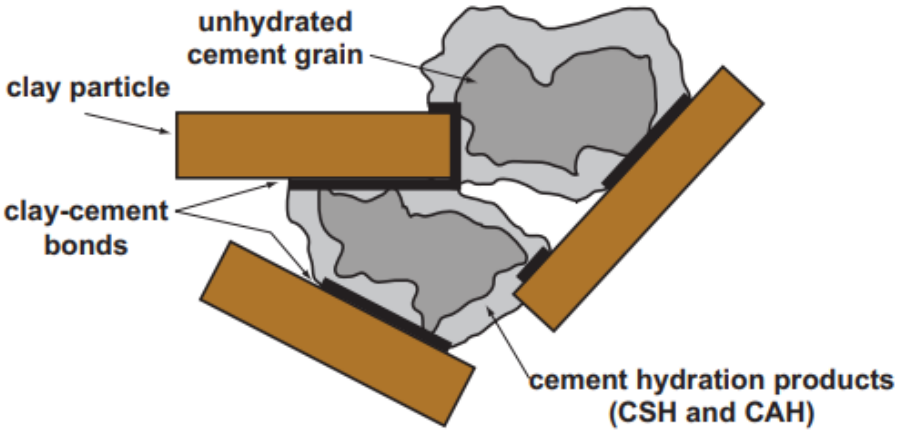

Figure 3: Cement hydration (Halsted et al. 2008)

Pozzolanic reaction

Additional C-S-H can occur in cement/lime-soil systems as a result of the reaction between Ca $(OH)_2$ supplied by either cement or lime and soil silica. This is referred to as a pozzolanic reaction. Calcium can also react with alumina in the soil to form C-A-H, which is a cementitious compound. This is shown in the following reactions;

$$Ca(OH)_2 + SiO_2 = C\text{-}S\text{-}H$$

$$Ca(OH)_2 + Al_2O_3 = C\text{-}A\text{-}H$$

where C = CaO, S = SiO_2, A = Al_2O_3 and H = H_2O.

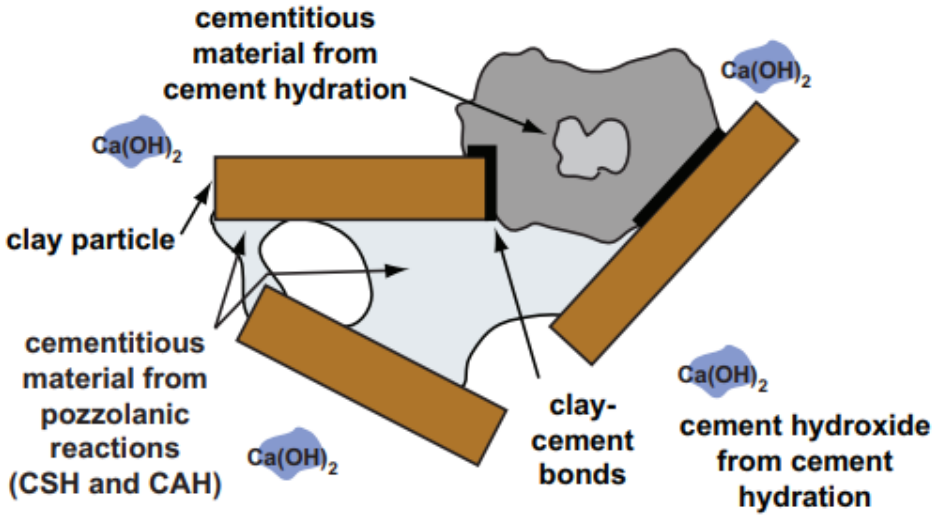

Figure 4: Pozzolanic reaction (Halsted et al. 2008)

1.6 The Need for Sustainable Binders

Soil stabilization with cementitious materials such as OPC and lime has been frequently used in construction to improve the strength of less competent soils. Massive globalization has resulted in skyrocketing demand for construction materials, contributing to the depletion of natural resources. Prolonged exploitation of raw materials and cement manufacturing causes material depletion and increases in global temperature by releasing surplus CO_2 into the atmosphere. Cement accounts for 8% of total anthropogenic carbon dioxide emissions. As a result, it is critical to develop novel and alternative stabilization materials to OPC and lime by using unconventional, more sustainable binders. Extensive research is needed in order test the feasibility of OPC alternatives for stabilizing soils to determine if they can improve the engineering properties of soils whilst minimizing environmental effects. For this reason, this thesis research focuses on the characterization of sustainable alternatives to OPC in soil stabilization and their feasibility as soil stabilizers.

CHAPTER 2 - CLASSIFICATION OF CLAYS AND BINDERS

2.1 Soil Classification

Soil is made up of a variety of mineral particles derived from rock fragments (2 mm in cross-section), fine grained minerals (particularly clay), organic matter, humus, soluble nutrients, living organisms, air voids, and water. Soil classification systems were developed to aid in the organization of soil knowledge. Many countries have national soil classification systems, however the two that are extensively used and adopted around the world are Soil Taxonomy and Soil Classification (Soil Survey Staff 1975) and the World Reference Base, IUSS Working Group WRB (2015). Soil Taxonomy is a hierarchical system that categorizes soils into six levels of detail, ranging from the most detailed level, soil series, to the broadest category, soil orders. The 12 Soil Orders at the broadest level are summarized in Table 1. Further information may be found in the Soil Survey Staff (1975), and the system is thoroughly documented on the website http://soils.cals.uidaho.edu/soilorders/orders.htm. Fig. 5 shows the global distribution of the 12 soil orders in Soil Taxonomy.

Table 1: Soil Taxonomy's 12 orders after Meyer J H (2013)

Class	Description
Gelisols	Soils with permafrost within 2 m of the surface.
Histasols	Soils containing a high organic matter content.
Spodosols	Acid forest soils with accumulation of metal-humus complexes in subsoil.
Andisols	Soils formed from volcanic ash.
Oxisols	Highly weathered subtropical and tropical soils.
Vertisols	Usually, black cracking clays with high shrink/swell potential.
Aridsols	Lime containing soils of arid environments
Ultisols	Strongly leached soils with clay accumulation in the subsoil with < 35 % base saturation
Mollisols	Grasslands soils with high base status.
Alfisols	Moderately leached soils with a subsurface accumulation of clay with > 35 % base saturation.
Inceptisols	Soils with weakly developed subsoils.
Entisols	Soils with little or no morpho-logical development

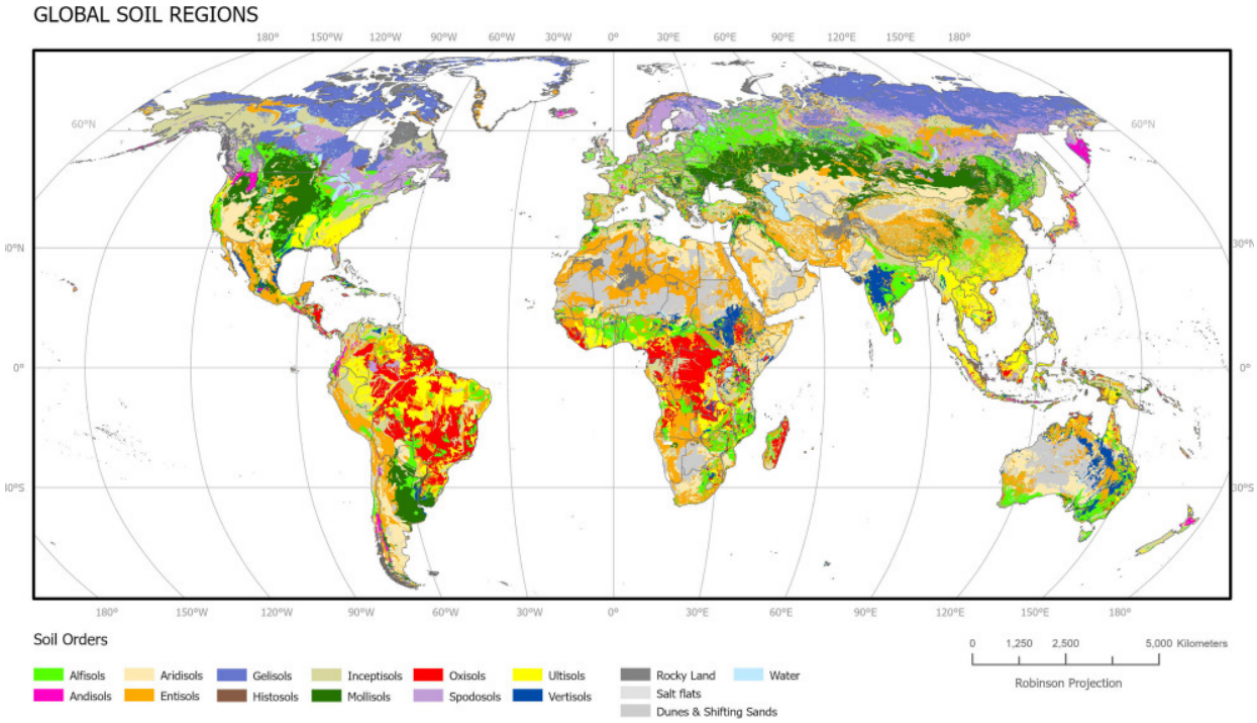

Figure 5: Global Distribution of Soils (Padmanabhan E et al 2022)

The most used classification method for engineering purposes is textural classification. This classification is based on particle size and percentage distribution. The relative proportions of different sized mineral particles in the soil are referred to as texture. The largest particle size diameter according to USDA standards includes gravel (> 2.0 mm), coarse sand (2.0–0.5 mm), medium sand (0.5–0.25 mm), fine sand (0.25–0.05 mm), silt (0.05–0.002 mm) and clay (< 0.002 mm) in diameter. Fig. 6 shows the textural classification of soils.

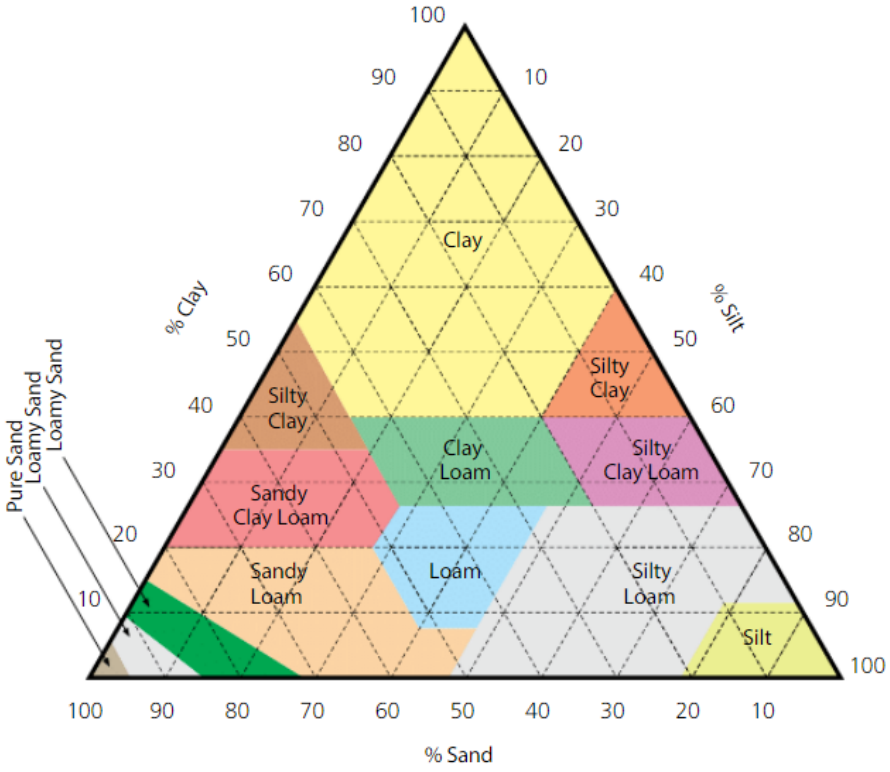

Figure 6: Soil Textural Classification Triangle (Meyer J 2013)

2.2 Clay Classification

Clay is a fundamental constituent of soil; it influences the physical and chemical properties of the soil. Clays are also important primary raw materials in the construction industry and in the production of cement. A clay is a naturally occurring material composed primarily of fine-grained minerals, which is generally plastic at appropriate water contents and will harden when dried or fired (Wypych F et al. 2022). Clays are mainly formed by phyllosilicates but may also contain other minerals such as quartz and various oxides and hydroxides. Phyllosilicates are a family of minerals containing continuous two-dimensional tetrahedral sheets of composition T_2O_5 (T=Si, Al, Be, …) with tetrahedra linked by sharing three corners of each, and with a fourth corner pointing in any direction. In the unit structure, tetrahedral sheets are linked to octahedral sheets, groups of coordinated cations, or individual cations. Clay minerals are typically composed of aluminum silicates, which are formed of tetrahedral and octahedral sheets that are collectively bound together via the sharing of apical oxygen atoms. Clay materials are formed in situ by alteration of rocks or surface weathering, hydrothermal action and weathering below the earth's surface.

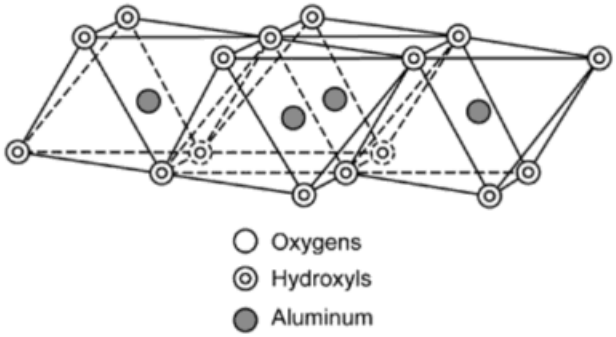

Figure 7: Diagrammatic sketch of an octahedral Sheet (Murray H 2007)

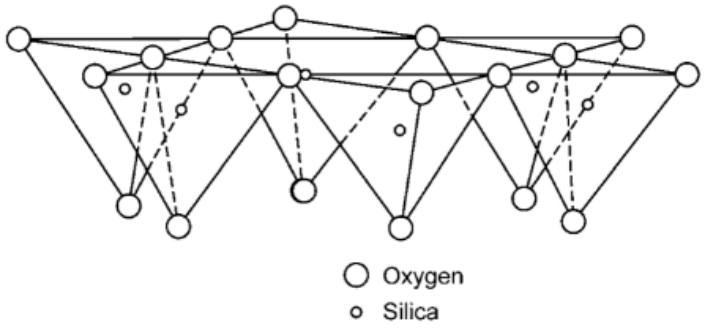

Figure 8: Diagrammatic sketch of a tetrahedral Sheet (Murray H 2007)

Clays are classified into three groups based on the number and arrangement of tetrahedral (silica) and octahedral (alumina-magnesia) sheets contained in the crystal units or layers as shown in Table 2.

Table 2: Sheets contained in the crystal units of clays

Group	d-spacing (Å)	Description
1:1	7	1 tetrahedral sheet 1 octahedral sheet
2:1	9-15	2 tetrahedral sheets 1 interposed octahedral sheet
2:2	14	1 T-O-T layer 1 brucitic octahedral sheet

Group 1:1 [T-O]

1:1 clay minerals are formed by combined tetrahedral and octahedral sheets in equal proportions. The sheets are held together by sharing common oxygen atoms. The apical oxygens of the silica tetrahedra are also octahedrally linked to the metal atoms.

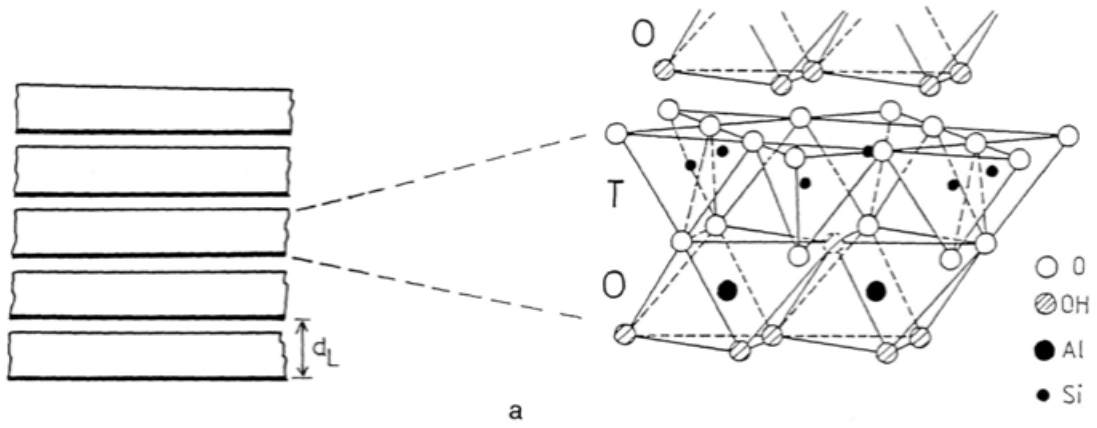

Figure 9: Structure of a 1:1 clay mineral (Jasmund K et al., 1993)

The serpentinite and kaolinite groups are examples of 1:1 type clays. The kaolinite group is the most common 1:1 type clay mineral which includes kaolinite, nacrite, dickite and halloysite. In the kaolin group minerals, the octahedral sheet is formed by aluminum atoms, in a structure analogous to γ-Al $(OH)_3$ or gibbsite (Ferreira E J et al. 2005). In the serpentine group minerals, the structure is made up of magnesium atoms instead of aluminum, in a structure analogue to Mg $(OH)_2$ or brucite (Ferreira E J et al. 2005). Only 2/3 of the octahedral sites in the aluminum sheet are occupied by metal atoms, resulting in a dioctahedral structure (with vacant octahedral sites) whereas all the octahedral sites are occupied in the Mg sheet, forming a trioctahedral structure. Because no excess charge is left unbalanced, the layers constructed in this manner are electrically neutral and as a consequence the layers can superimpose each other (stacking). Cations and water do not enter between the structural layers of a 1:1 type mineral particle, so kaolinite does not adsorb water in the interlayer. Kaolinite exhibits very little cohesion, shrinkage, swelling, or plasticity (ability to be molded).

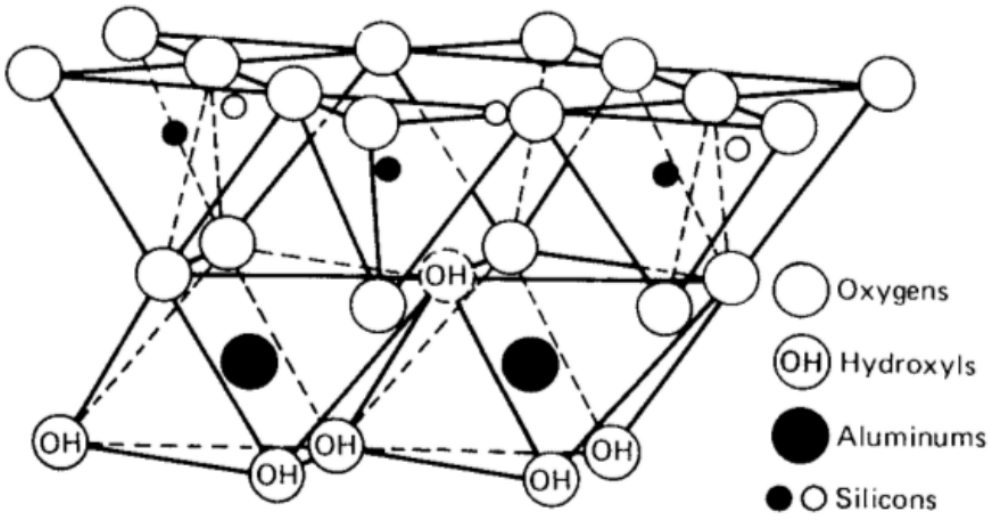

Figure 10: Diagrammatic structure of a kaolinite mineral (Mitchell and Soga 2005)

Group 2:1 T-O-T

These minerals' crystal units (layers) are defined by an octahedral sheet sandwiched between two tetrahedral sheets. Three general groups have this crystal structure. The 2:1 type clays can be further subdived into the following:

- Expanding Type: Smectite group and Vermiculite.
- Non-expanding Type: Mica group.

a) Expanding type

The smectite group, which includes montmorillonite, beidellite, nontronite, saponite and hectorite is noted for its interlayer expansion and extensive swelling when wetted. The most common smectite is montmorillonite, which has a general chemical formula: $(1/2Ca,Na)(Al,Mg,Fe)_4(Si,Al)_8O_{20}(OH)_4$. The octahedral substitution of Mg^{2+} for Al^{3+} gives montmorillonite its charge. As the mineral hydrates, the presence of exchangeable cations in the interlayer between water molecules causes the crystal lattice to expand. When the material is saturated with water, the basal spacing between layers can exceed 2 nm, but it can be reduced to less than 1 when the mineral is dry. This smectite expansion and contraction trait, also referred to as shrink-swell potential, is problematic to engineers due to the strong tendency for crack formation and general soil surface instability.

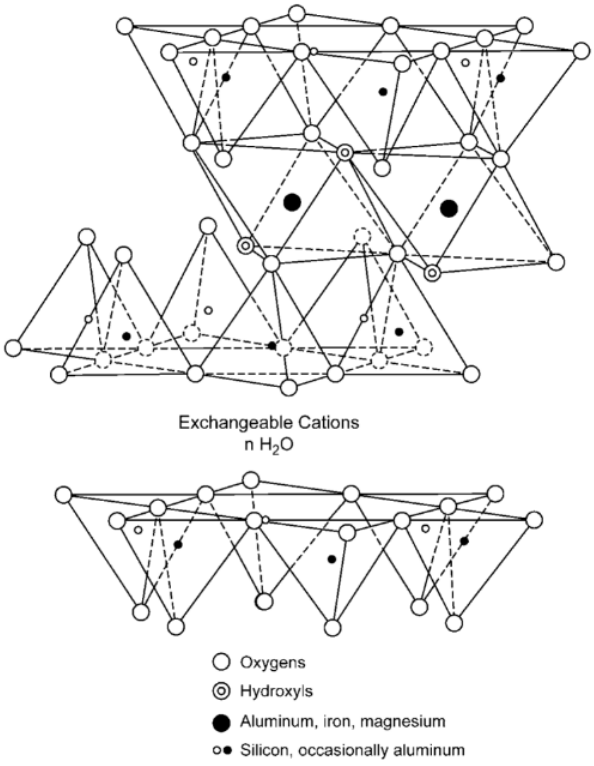

Figure 11: Diagrammatic structure of a smectite mineral (Murray H 2007)

Vermiculite which is generally a weathering product of mica is a highly charged 2:1 clay. It has a layer charge per unit cell of between 0.6-0.9. Due to the tetrahedral charge origin, water molecules and exchangeable cations primarily Mg^{2+} and Ca^{2+} are highly adsorbed within the interlayer region of vermiculites. Since the presence of hydration water is only achievable due to the layers' relatively low negative charge, expandable vermiculite can only be obtained after heat treatment, with the particles expanding around 30 times their original size. (Wypych F et al. 2022)

b) Non-expanding type

Micas e.g. muscovite and biotite are the typical minerals in this group. The tetrahedral sheet is the primary source of charge, with aluminum atoms occupying approximately 20% of the silicon sites, resulting in a net negative charge in the tetrahedral sheet. To compensate this charge, potassium or occasionaly calcium and magnesium ions are strongly attracted to the interlayer space and are just the right size to fit into the adjacent tetrahedral sheets' spaces. The interlayer cations of K, Ca, or Mg prohibit water from entering the structure. As a result, the micas are non expanding.

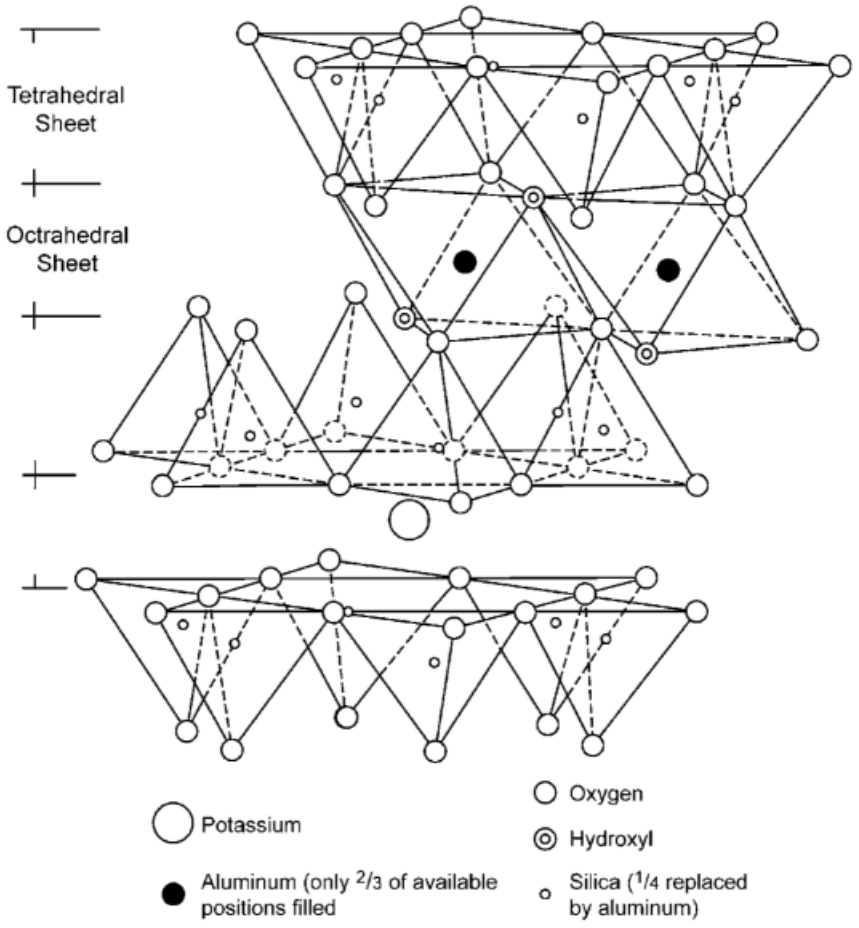

Figure 12: Diagrammatic sketch of illite (Murray H 2007)

Group 2:2

This group is represented by chlorites. Chlorites are hydrous aluminosilicates with a 2:1 interlayer structure. Contrary to other 2:1 clay minerals, the interlayer spaces of chlorite are occupied by hydroxides of Mg^{2+}, Al^{3+}, or Fe^{3+} resulting in a 2:1:1 structure, as shown in the Fig. 13 The absence of water adsorption between chlorite crystal units explains why this mineral does not expand. Chlorite is generally intimately intermixed with other clay minerals so it can be identified by the 14 Å basal spacing which does not expand when treated with ethylene glycol nor decrease to 10 Å upon heating (Murray H et al. 2007).

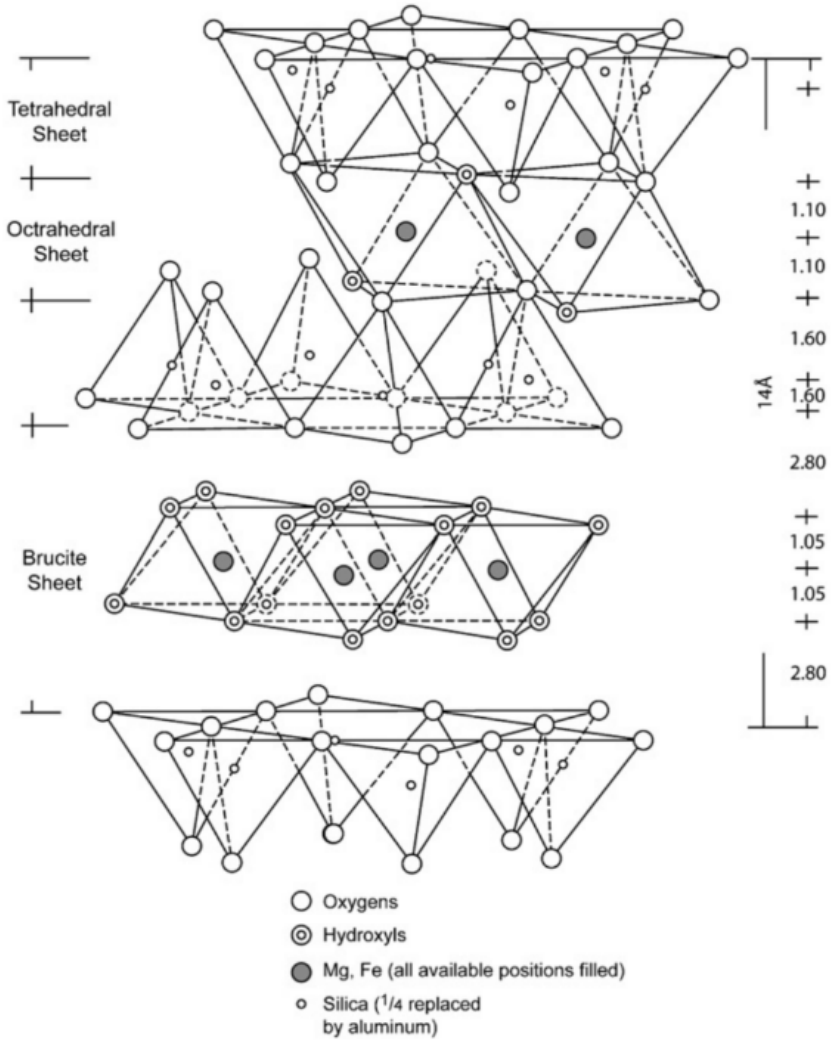

Figure 13: Diagrammatic sketch of a chlorite structure (Murray H 2007)

2.3 Cement Classification

a) Ordinary Portland Cement

Cement is a hydraulic binder, which when mixed with water forms a paste that sets and hardens by means of hydration reactions and processes; and which after hardening retains its strength and stability even under water (British Standards BS 12). The presence of water commonly aids the reactions that are involved. The origins of Portland cement can be traced back to Greek and Roman times, but the year 1824 is widely regarded as the year when the name "Portland" was used in a patent by Joseph Aspdin to exemplify the similarity of concrete made with his cement to Portland limestone, which was a popular material for construction at the time. Nowadays, Ordinary Portland Cement is the most commonly used cement type for construction purposes. It is one of the largest consumed products besides water. According to estimates, the total mass of cement production worldwide was 4.1 billion tonnes in 2022. The total global cement production

in 1995 was only 1.39 billion tons, demonstrating the extent to which the construction industry has grown since then (Statista 2023).

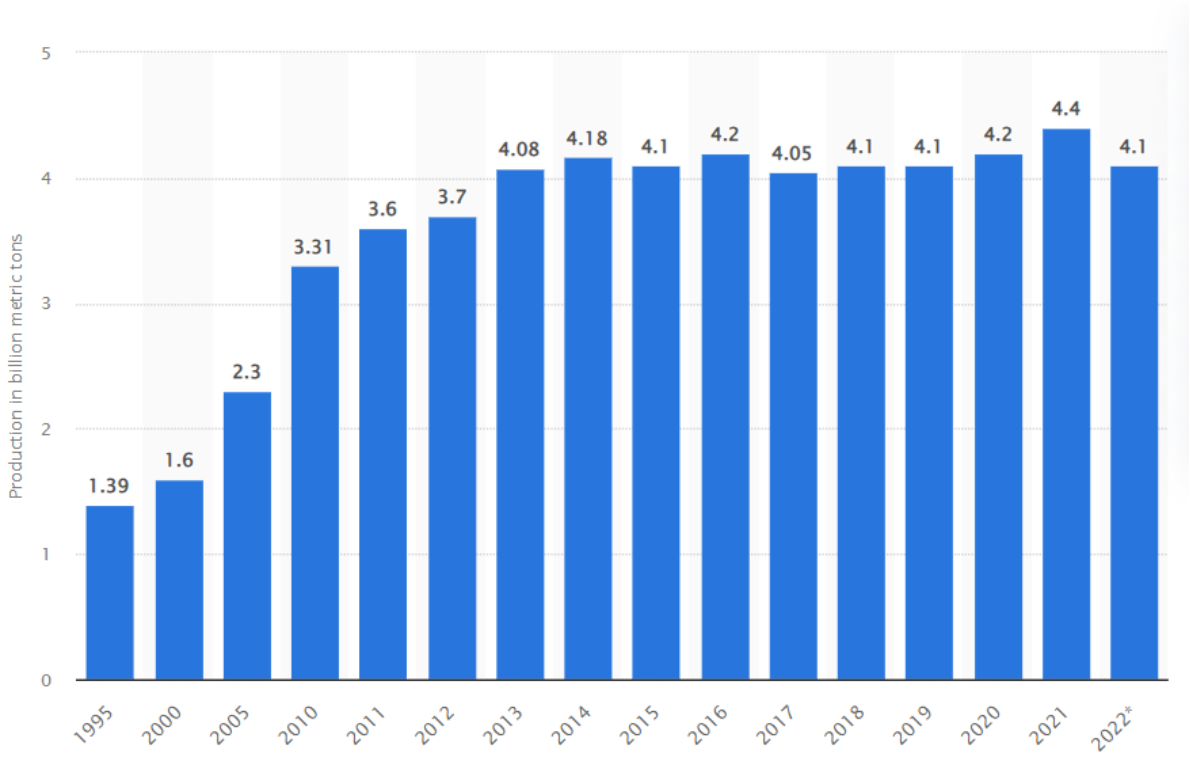

Figure 14: Cement Production Worldwide from 1995-2022 (Statista 2023)

Cement production

More than 30 raw materials are known to be utilized in the manufacture of portland cement, which can be classified into four types: calcareous, siliceous, argillaceous, and ferriferous. The main constituents are limestone ($CaCO_3$) and silica (SiO_2), coming from sources such as clay and sand, which when heated to high temperatures (1450°C) form the hydraulic calcium silicates and aluminates, which are the active compounds in cement. The first step in the manufacturing of Portland cement is the acquisition of raw materials. Calcium, the most abundant element in Portland cement is derived from a variety of calcareous raw materials, including limestone, aragonite, marl, sea shells and chalk.

The second step in manufacturing Portland cement is crushing the raw materials. In facilities using the dry process, the moisture is normally decreased to less than 1% by dryers, air seperators or impact mills. The dried material is then blended and transported and stored in silos until it is fed to the pyroprocessing system. In facilities using the wet process, during the raw material grinding process, water is fed to the raw mill producing a slurry of about 65% solids. The slurry is then blended and transported in cylindrical tanks until it is fed to the pyroprocessing system.

The third step in the manufacturing of Portland cement is burning in a rotary kiln at high temperature which transforms the raw material into clinkers. Clinkers are gray, glass-hard, spherically formed nodules that range in size from 0.32 to 5.1 centimeters (cm) in size. This stage can be sequentially summarised as follows;

- Evaporation of free water as the tempratures increase upto 100°C;
- Calcination of calcium carbonate ($CaCO_3$) to calcium oxide (CaO);
- Reaction of CaO with silica to form dicalcium silicate (1450-1500°C);
- Reaction of CaO with aluminum and iron-bearing constituents to form the liquid phase;
- Reaction, of oxides in the burning zone of the rotary kiln, to form cement clinker at temperatures of approximately 1510°C.
- Reaction of excess CaO with dicalcium silicate to form tricalcium silicate.

It is during this proprocessing that fuels are combusted to produce energy which releases substantial quantities of CO_2. Significant amounts of CO_2 are also produced during the calcination of limestone or other calcareous material. $CaCO_3$ is thermally decomposed to CaO and CO_2 during the calcining process.

The final stage in the manufacture of Portland cement is the blending and grinding of the clinker to form portland cement. Small amounts of Gypsum (upto 5%) are added at this stage to prevent early hydration of C_3A thus optimizing cement perfomance. The overall process is shown schematically in Fig. 15.

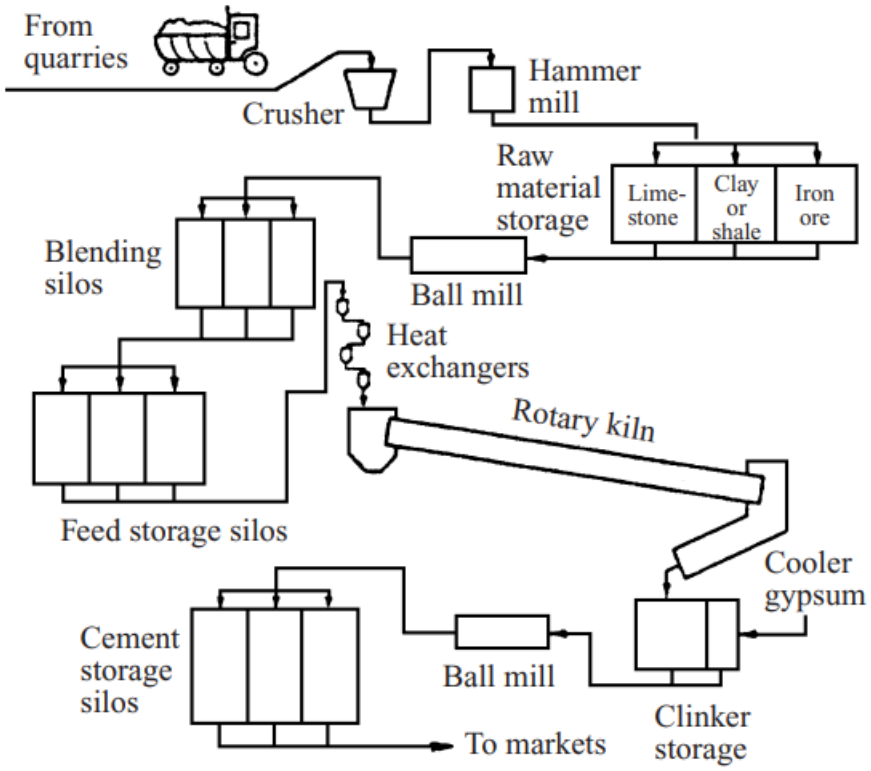

Figure 15: Schematic representation of cement manufacturing (Young J F 2001)

Chemical composition of OPC

Table 3 lists the chemical components of Portland cement (Ali et al., 2008). Physical property variations in cement occur as a result of changes in the amount of chemical constituents.

Table 3: Chemical components of Portland cement

Component	Amount
Lime (CaO)	60-70%
Silica ($Si0_2$)	17-25%
Alumina (Al_2O_3)	3-8%
Iron Oxide (Fe_2O_3)	0.5-6%
Magnesia (MgO)	0.1-4 %
Sulphur trioxide (SO_3)	1-3%
Soda and/or Potash (Na_2O+K_2O)	0.5-1.3%

Burning and fusion cause chemical reactions among the components of raw materials, to produce clinker phases. Portland cement is made up of four major clinker compounds: C_3S, C_2S, C_3A, and

C_4AF, as well as gypsum added during the grinding process. The relative proportions of these compounds can be changed to optimize specific properties of the cement (Young J F 2001).

C_3S (Alite)

It constitutes 50-80% of Portland cement. Alite has seven polymorphs (3 triclinic, 3 monoclinic, 1 rhombohedral). Portland cement frequently contains monoclinic polymorphs. Its structure may contain minor impurities of Mg, Al, and Fe. It reacts more rapidly with water than C_2S.

C_2S (Belite)

Five polymorphs make up the Belite structure (3 orthorombic, 1 monoclinic, 1 hexagonal). The most prevalent polymorph in Portland cement is monoclinic, and it can accommodate trace amounts of cations. At ambient temperatures, the nonhydraulic γ polymorph is thermodynamically stable however impurities, in cement stabilize the hydraulic β polymorph (Young J F 2001).

C_3A (Aluminate)

The Aluminate structure can either be cubic/orthorombic. The cubic polymorph is the most common in Portland cement. Impure C_3A contains a significant amount of iron (approximately 10 mol.%), which may make it less reactive than the pure compound. High levels of sodium substitution change its crystal structure from orthorhombic to cubic, resulting in a decrease in reactivity.

C_4AF (Ferrite)

The composition of the ferrite phase is close to C_4AF in many cements, it is closer to C_6AF_2 in those with very low C_3A contents. The reactivity of the ferrite phase decreases as the iron content increases.

Minor phases

Other minor phases found in Portland cement are periclase (MgO), free lime (CaO), portlandite ($Ca(OH)_2$) and alkali sufates such as arcanite. Caution should be take about the limits of MgO and CaO because its slow hydration can cause disruptive expansions in the hardened cement paste.

Cement hydration

Cement sets and hardens as a result of complex chemical reactions between cement and water (hydration) in the cement paste binder (Young J F 2001). Different clinker phases have different reactivity with water. Table 4 summarizes the overall reactions.

Table 4: Summary of the overall reactions of clinker phases

Compound	Hydration reactions	Heat of reaction	
		kJmol-1	Jg-1
Alite	$2C_3S + 11H = C_3S_2H_8 + 3CH$	-114	-500
Belite	$2C_2S + 9H = C_3S_2H_8 + CH$	-43	-250
Aluminate	$C_3A + 3CSH_2 + 26H = C_6AS_3H_{32}$	-365	-1350
Ferrite	$C_4AF + 15H = C_4(A_3F)SH_{12} + (A,F)H_3$	-403	-200

C_3S is the main constituent of Portland cement, and its hydration contributes significantly to the development of mechanical strength at early ages of hydration. The hydration of belite (C_2S) is analogous to that of alite (C_3S) but at a slower rate. The hydration products from both are an amorphous calcium silicate hydrate (C-S-H) and crystalline calcium hydroxide (CH). Since the composition of the calcium silicate hydrate is variable, it is usually referred to as C-S-H which implies no definite stoichiometry. The hydration of C_3S is largely exorthemic. The alite content controls the development of strength during the first seven days.

Calcium sulfoaluminate hydrates are formed in the presence of gypsum by C_3A and the ferrite phase. The first product to be formed is ettringite ($C_6AS_3H_{32}$), a trisulfate aluminium hydrate, but when all of the gypsum is consumed, ettringite converts to calcium aluminate monosulfate (AFm phases or Al_2O_3, Fe_2O_3-mono). Despite their minor strength contributions, C_3A and the ferrite phase are however significant compunds. In the absence of gypsum, C_3A reacts rapidly with water, forming calcium-aluminate hydrates with varying compositions . These calcium aluminate hydrates are globally known as alumina-ferric oxide monosulfate (AFm phases).This extremely rapid reaction determines the paste's 'flash set' (instantaneous stiffening).

Hydration of the ferrite and aluminate phases are similar. Fe can replace a part of Al in ettringite and monosulfate, and the phases formed from substitution of pure ettringite and monosulfate are the alumina-ferric oxide trisulfate (AFt) and alumina-ferric oxide monosulfate (AFm). The rate of hydration for the reactions involving the various clinker phases, and gypsum, are shown in Fig. 16.

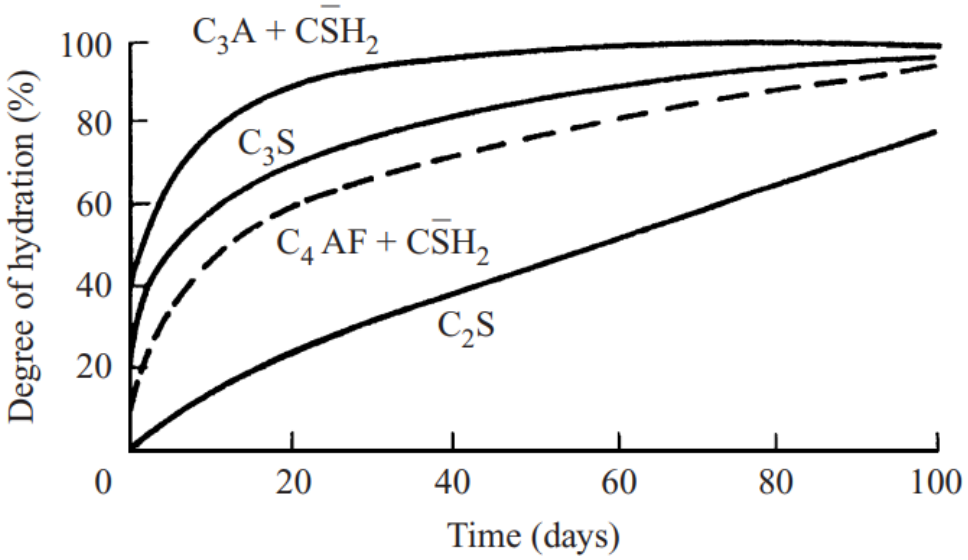

Figure 16: Rate of hydration of clinker compounds (Young J F 2001)

b) Limestone calcined clay cement (LC^3)

LC^3 is cement made of a blend of limestone and calcined clay mixed in the proportions of 5% gypsum, 15% limestone, 30% calcined clay and 50% Portland clinker as shown in Fig. 17. Limestone calcined clay cement (LC^3) was first proposed by the Ecole Polytechnique de Lausanne (EPFL) in an effort to reduce carbon emissions and maximize resource efficiency in cement production. Limestone calcined clay cement (LC^3) can attain comparable strength to Ordinary Portland Cement (OPC) with clinker content as low as 50% thereby reducing the carbon footprint associated with the cement industry.

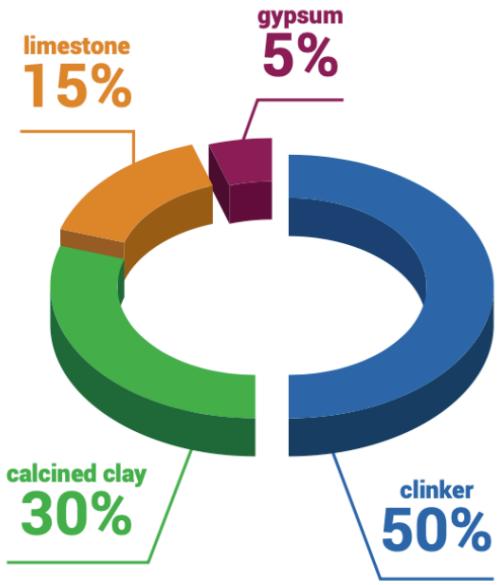

Figure 17: LC3 composition (https://lc3.ch)

Supplementary cementitious materials (SCMs) are soluble siliceous, aluminosiliceous, or calcium aluminosiliceous powders that are used as partial replacements for clinker or portland cement in cements. The use of supplementary cementitious materials (SCMs) in cement manufacturing has a significant potential to minimize carbon emissions by reducing the amount of clinker used and virgin resource usage, particularly in developing nations. 95% of traditional Portland cement comprises of clinker. Its manufacture is energy-intensive and accounts for a large portion of anthropogenic CO_2 emissions . Using Supplementary Cementitious Materials (SCMs) a reduction in CO_2 emissions can be achieved. LC^3 can reduce half of the clinker content (Fig. 18) and thereby cut up to 40% of the CO_2 emissions.

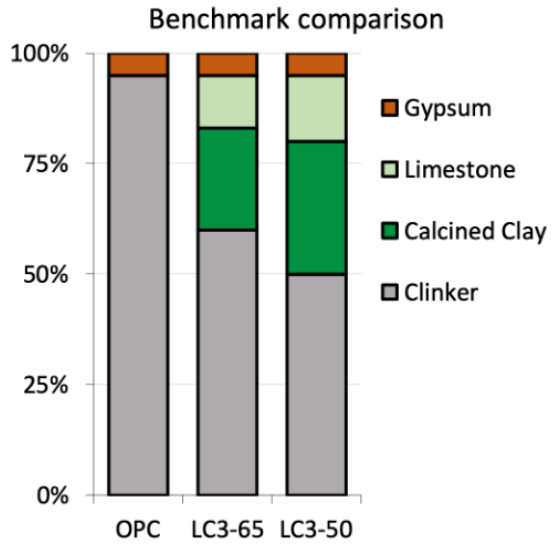

Figure 18: Comparison between OPC and LC3 (https://lc3.ch)

The main problem with the usage of suplementary cementetious materials (SCM's) is limited supply e.g. silica fume and blast furnance slag, which prevents them from being used in large scale cement production. Clays, on the other hand, are abundant worldwide (Ahmed Z K et al. 2020). Clays and limestone are among the most abundant materials in the earth's crust. The global availability of SCM's is shown in Fig. 19.

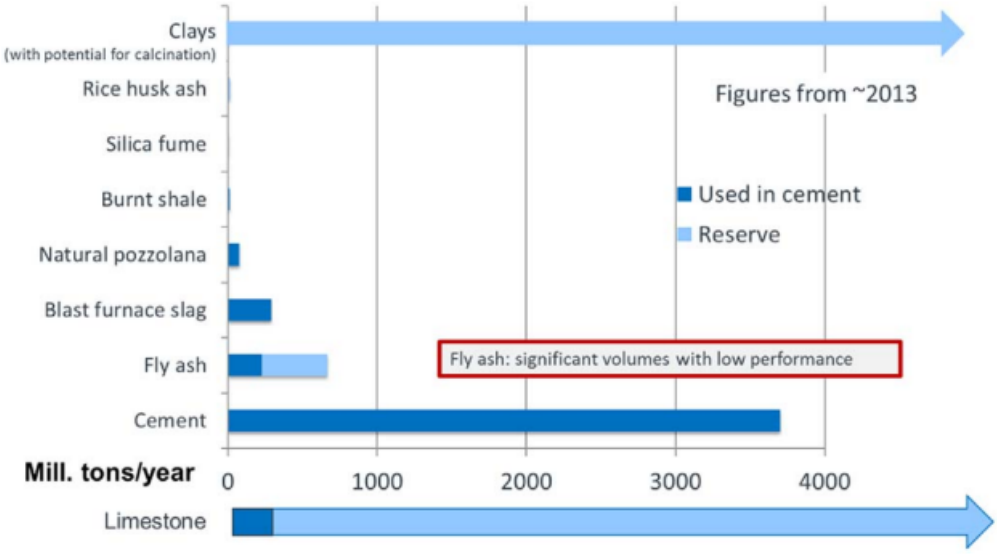

Figure 19: Availability of SCM's (Scrivener K et al. 2018)

Clays may contain a large amount of kaolinite and have been shown to be significantly pozzolanic when calcined between 700 and 850°C (Fernandez R et al. 2011). Thermal activation at appropriate temperatures can eliminate the structural water in the clay; this process is known as dehydroxylation. The removal of structural water from kaolinite may lead it to transition into a metastable state with higher structural disorder, known as metakaolinite, as show in Fig. 20.

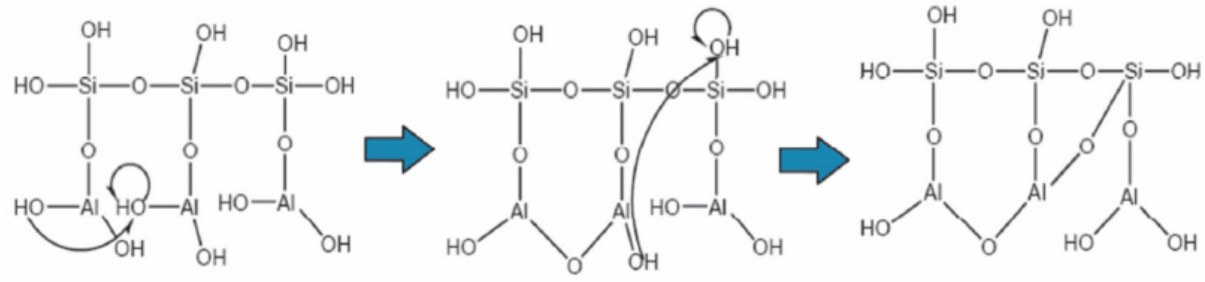

Figure 20: High reactivity clays to form calcined clays (Zhao Y et al. 2023)

Metakaolin ($Al_2Si_2O_7$) is a highly reactive pozzolan formed by the calcination of kaolinite-rich clays. The pozzolanic reaction of metakaolin with the calcium hydroxide (CH) forming during the hydration of Portland cement is show below;

$$AS_2 + 5CH + H = C_4AH_{13} + 2\ C\text{-}S\text{-}H$$

Metakaolin + Calcium Hydroxide + Water = Calcium Aluminate Hydrate + Calcium Silica Hydrate

Metakaolin is rich in lumina hence its use increases the volume of alumina rich phases in the system. When Limestone is added, the Calcium Carbonate (Cc) reacts with the alumina phases to form monocarboaluminate (Mc) and hermicarboaluminate (Hc).

$$C_3 + C_c + 11H = C_4ACH_{11} \qquad \text{Monocarboaluminate}$$

$$C_3A + 0.5C_c + 0.5CH + 11.5H = C_4AC0.5H_{12} \quad \text{Hermicarboaluminate}$$

On the basis of these reactions a fraction of clinker can be replaced by a similar proportion of metakaolinite and calcium carbonate mixed in a 2:1 ratio to generate hydration products that can fill the pore space of the cement matrix and contribute to its strength and durability. Pure kaolins contain large amount of kaolinite making them more expensive because of the competition over them with other sectors hence the use of medium purity kaolins. Medium purity kaolinite clays have also shown to be a good substitute for metakaolinite.

Effect of calcined clay on cement hydration

The metakaolin formed from calcining clay may potentially accelerate cement hydration due to its higher surface area for heterogeneous nucleation. Metakaolin is easily attacked by hydroxyl ions in the pore solution of ordinary cement and dissolved as a result.

$$Al_2O_3(SiO_2)_2 + 6OH^- + 3H_2O \rightarrow 2Al(OH)_4^- + 2H_2SiO_4^{2-}$$

As the aluminum concentration increases in the solution, the aluminum incorporation into C-A-S-H increases accordingly, and the equation is as shown below;

$$2AS_2 + 9CH + 12H \rightarrow C_2ASH_8 + C4AH13 + 3CSH$$

CHAPTER 3 - PRELIMINARY ANALYSIS

This chapter explains the results of a preliminary analysis that was conducted at the Meru University of Science and Technology, Kenya, within a partnership into this project. Such preliminary analyses, carried out by the partner institution, examined the geotechnical properties of the samples used in this study when stabilized by LC^3 and OPC. The results are briefly summarised in this chapter to provide some background for the rest of the experimental study carried out within this thesis project.

3.1 Atteberg Limits

The Atteberg limits define the general consistency of the soil (i.e. the range of water concentrations at which the soil transitions from solid, to plastic, to liquid behaviour), Fig. 21.

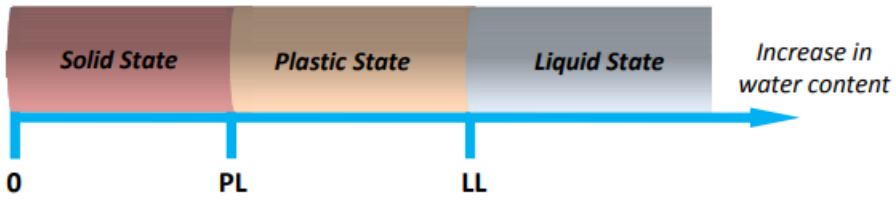

Figure 21: Atterberg Limits (J Kisunge, 2012)

The limits determined include:

- Plastic Limit: the minimum moisture content sufficient to transform a soil from solid (dry) to plastic (mouldable) state.
- Liquid limit: the moisture content that causes soil to transition from a plastic state to a liquid state.
- Plasticity index: the moisture content range at which soils remain plastic (mouldable). It is calculated mathematically as the difference between the liquid and plastic limits (PI = LL - PL).
- Linear shrinkage: the decrease in length of a wet soil after drying. As wet soil dries, it simulates the volumetric changes that occur.

3.2 Proctor Test

The proctor test is laboratory compaction method for demonstrating the relation between moisture content and density of a substance (compacted mass of material in a unit volume throughout a range of moisture contents).

3.3 California Bearing Ratio

This is a test used to determine the strength of subgrade soil and pavement layers. It determines the load-bearing capacity of soils used for construction purposes.

The clay used in the study was found to have the properties listed in Table 5 which proved it to be a highly plastic clay.

Table 5: Properties of the clay used in this study

Property	Value	Standard
% Passing 0.075 mm sieve	69.2	Max 50
Liquid limit (%)	66	Max 50
Plastic Limit (%)	29.6	-
Plasticity Index (%)	36.4	Max 25
Optimum Moisture Content (%)	23.6	Max 20
Maximum Dry Density (kg/m3)	1558	Min 1400
Califonia Bearing Ratio (%)	7	-
pH	5.46	Min 5.30
Organic Content (%)	1.83	Max 2
Sulphate Content (ppm)	1671.7	Max 3000
AASHTO Classification	A-7-6	
USCS	CH	

From the Atterberg limits analysis (Fig. 22), it was found that the optimum ratio for LC^3 to soil was 5% so this was the ratio used for the rest of the tests. The Atterberg limits are the best determinant for the cement ratio to be used.

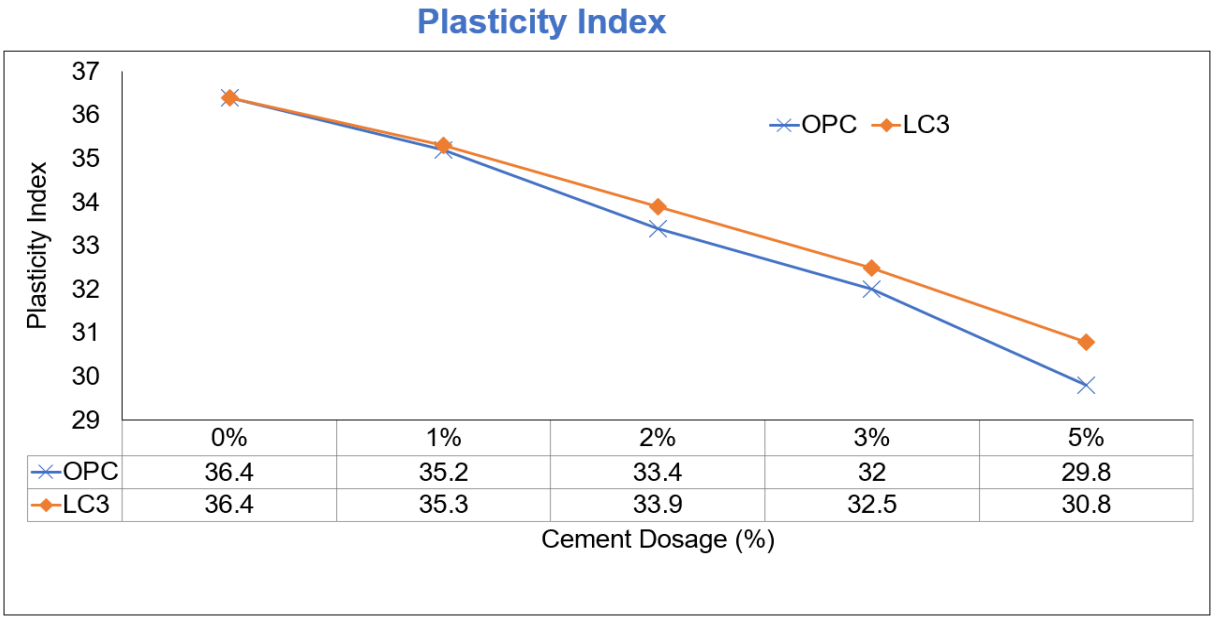

Figure 22: Effect of OPC and LC^3 on Plasticity Index of the Clay Soil

To reduce the plasticity of the clay and make it suitable for use in cement, quarry dust was added. Quarry dust reduces the clays' fine content thereby reducing its surface area and consequently its plasticity. A clay to quarry dust ratio of 50:50 and 60:40 was used and both ratios met engineering reqiurements for building purposes though the 60:40 ratio is preferred for economic purposes hence this was the ratio used for this study.

The atterberg limits showed that both the 60:40 and 50:50 ratios worked well for both OPC and LC^3. The plasticity index, linear shrinkage and liquid limit all decreased with increasing cement dosage, with the optimum cement dosage being 5% as it had the lowest limit for all 3 limits. This indicates that the plasticity had been adequately reduced resulting in minimum shrinkage Fig. 23. Fig. 24 also shows a great decrease in the plasticity index after stabilization from 36.4 to approximately 11.5% for OPC and 12% at a 60:40 ratio.

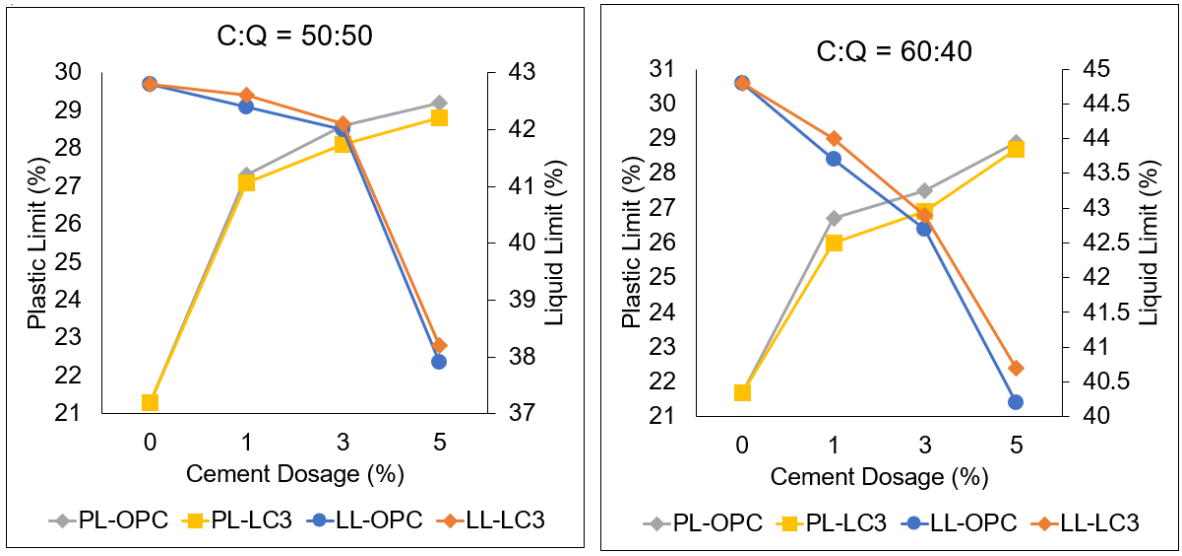

Figure 23: Plastic and Liquid Limit for stabilized soil

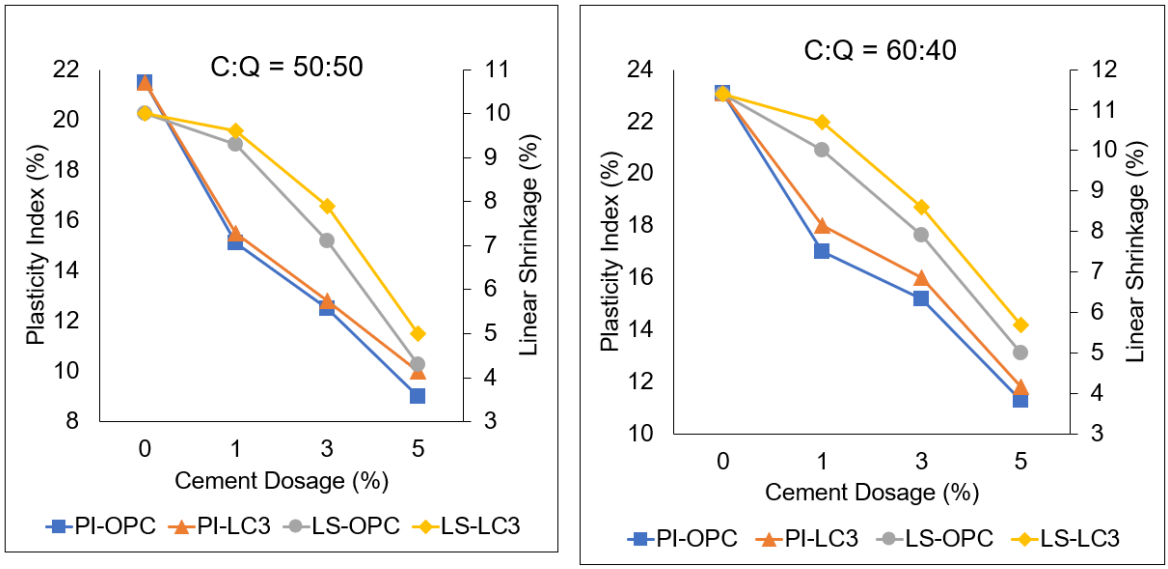

Figure 24: Plasticity Index & Linear Shrinkage for stabilized soil

The proctor test is an effective way to determine if stabilization has occurred, as it shows an increase in density and a reduction in moisture content which is due to an increase in compaction

of the soil particles. Fig. 25 showed that as the cement dosage increased for both LC^3 and OPC at both 50:50 and 60:40 ratios, the maximum dry density increased resulting in a gradual reduction of the moisture content.

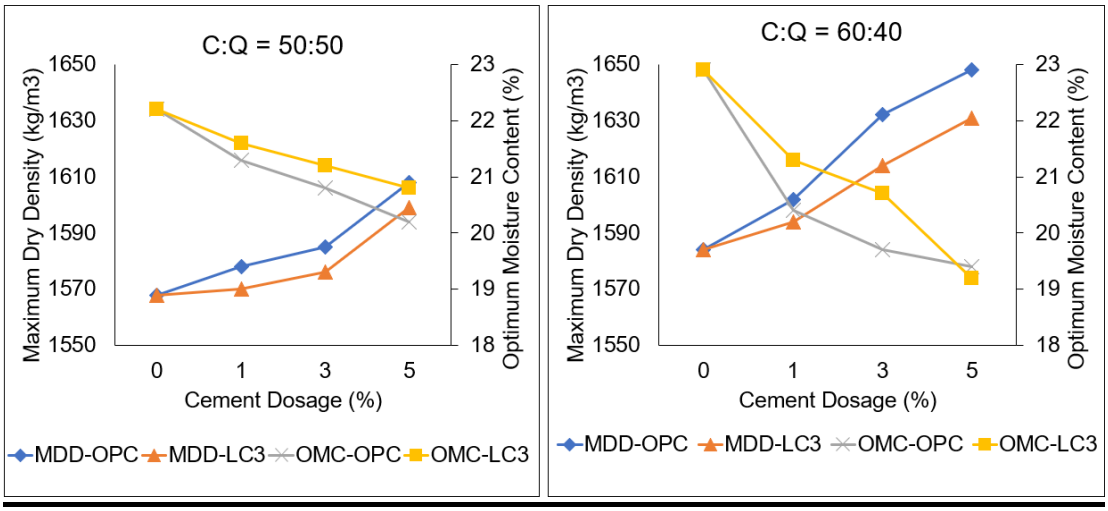

Figure 25: Proctor test results

The results from the California bearing ratio for both OPC and LC^3, at 50:50 and 60:40 ratios, show that the load bearing capacity of the soil was increased after stabilization. The increase in strength was due to the formation of the hydration products C-S-H and C-A-H which bind the cement matrix. As the CBR test was perfomed after 14 days, OPC perfomed better because than LC^3, because the pozzolanic reaction occurring in the latter occur with a slower rate. Addition of a cement dosage of 3% met the minimum strength requirement of 80% (O'Flaherty A C et al. 1961).

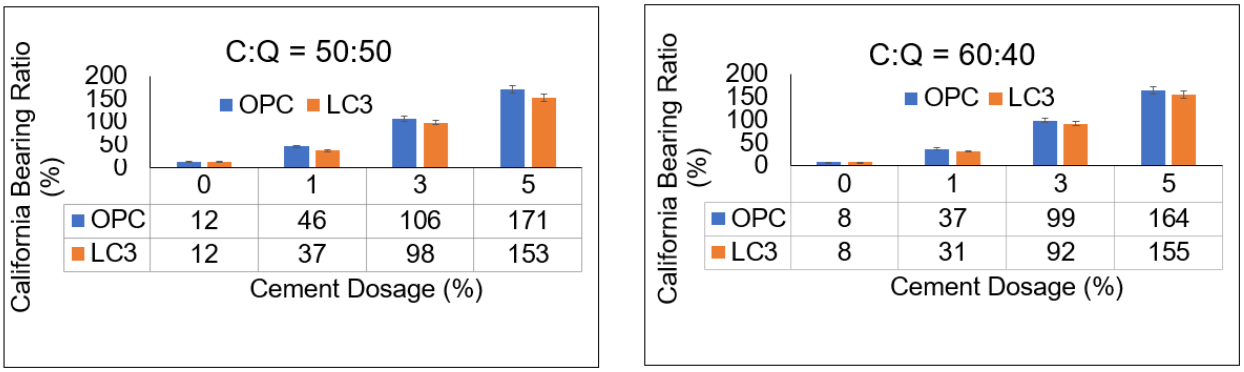

Figure 26: CBR results perfomed after 14 days of curing

LC^3 cement was found to be a suitable alternative to OPC because the overall performance was comparable for all the tests conducted.

CHAPTER 4 - MATERIALS

This chapter describes the samples used in this study, how they were prepared and where they were collected.

4.1 Materials

The clay soil utilized in this study was sourced from Meru, Kenya, at the geographical coordinates (0˚8’ 5.4056" N, 37˚ 42’ 29.76616" E). To remove the organic matter-containing subsoil, the clay soil was dug out from three locations 50 m apart at a depth of 50 cm from the ground's surface. 100 kg of soil were collected from each site and thoroughly mixed to produce a 300 kg mixture, which was then air-dried for 24 hours. The air dried soil was placed in ten airtight sacks and kept at room temperature in the laboratory. Quarry dust was collected from Meru, Kenya, at the geographical coordinates 0˚ 01'29.6"S, 37 ˚37'14.9"E. The cement (CEM 1) was obtained locally.

4.2 Preparation of the LC^3

In accordance with the preparation description given by Scrivener et al. (2018), LC^3 was prepared by grinding clay, clinker, limestone and gypsum seperately in a laboratory ball mill. It was then mixed in percentages of 50% Portland clinker, 30% calcined clay, 15% limestone, and 5% gypsum. The OPC and LC^3 cements used in this study had the following chemical composition (Table 6)

Table 6: Chemical composition of the OPC and LC^3 used in this study

Component	OPC (%)	LC3(%)
SiO_2	20.24	29.39
Al_2O_3	4.98	10.40
Fe_2O_3	3.96	2.79
CaO	63.00	44.34
MgO	1.23	0.84
SO_3	1.77	1.85
K_2O	0.71	0.57
Na_2O	0.18	0.26
P_2O_5	0.11	0.10
TiO_2	0.32	0.53
Mn_2O_3	0.09	0.08
Cl	0.02	0.00
L.S.F	0.98	0.44
Insoluble Residue (%)	3.98	28
$CaO+SiO_2$	83.34	73.73

4.3 Mineralogical Characterization of the Soil

Following California bearing ratio (CBR) determination, non-disintegrated sections of the CBR specimen cured for 14 days were taken from the top, middle, and bottom parts for XRD, SEM, and TGA analysis. To end hydration, the samples were immersed in isopropanol for 48 hours before being oven-dried at 40˚C for 30 minutes. The neat clay and quarry dust were then mixed using a ratio of 60:40 (Chapter 3) with 1%, 3% and 5% OPC or LC^3 as shown in Table 7.

Table 7: Sample packing for this study

Sample Code	Mass	Description (Neat Clay Soil: Quarry Dust = 60:40)
S1	250g	Neat LC3 (unhydrated)
C	100g	Neat Clay soil
Q	100g	Neat Quarry Dust
M0	100g	Neat Clay: Quarry dust Mixture (60:40)
M1	60g	60:40 Mixture stabilized with 1 % LC^3
M2	110g	60:40 Mixture stabilized with 3 % LC^3
M3	120g	60:40 Mixture stabilized with 5 % LC3
M4	110g	60:40 Mixture stabilized with 1 % OPC
M5	150g	60:40 Mixture stabilized with 3 % OPC
M6	100g	60:40 Mixture stabilized with 5 % OPC

CHAPTER 5 - EXPERIMENTAL TECHNIQUES AND METHODS

This chapter describes the different techniques used in this study from a theoretical point of view and the methodology used.

5.1 X-Ray Diffraction (XRD)

XRD is an analytical technique that irradiates a polycrystalline sample using an X-ray (monochromatic X-ray beam) and evaluates the diffraction effects. It is used for quantitative analysis, phase identification, crystal structure and microstructure analysis of materials. Non amorphous materials, such as minerals, have a three-dimensional structure that is determined by the regular, repeating planes of their atoms in a way that can be mathematically described. When a focused X-ray beam interacts with these planes of atoms, it is partially transmitted, absorbed by the sample, refracted and scattered, and diffracted. In XRD, X-rays are generated in a sealed tube that is under a vacuum. A filament within a tube is heated up by an applied current, the higher the current, the greater the number of electrons emitted. An X-ray diffractometer's geometry is such that the sample rotates at an angle θ in the direction of the collimated X-ray beam, while the X-ray detector is positioned on an arm to collect the diffracted X-rays and rotates at an angle of 2θ. A goniometer is the instrument used to maintain the angle and rotate the sample.

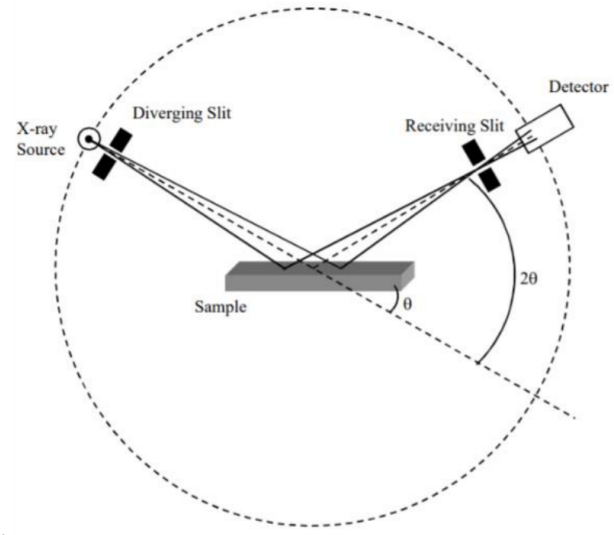

Figure 27: Schematic representation of a diffractometer (Kocak A 2018)

The technique is often employed in cement for qualitative analysis, such as phase identification and quantitative phase analysis (QPA), to determine the concentration of (hydrated) cement phases. During an XRD experiment, X-rays are diffracted by the crystalline material and an XRD pattern of varying intensities at particular diffraction angles is produced. The incident rays'

interaction with the sample produces constructive interference (and a diffracted ray) when conditions satisfy Bragg's law (Bunaciu A et al. 2015):

$$n\lambda=2d_{hkl}\sin\theta$$

where n is an integer, λ is the wavelength of the X-rays, d_{hkl} is the interplanar spacing of the plane hkl generating the diffraction and θ is the diffraction angle.

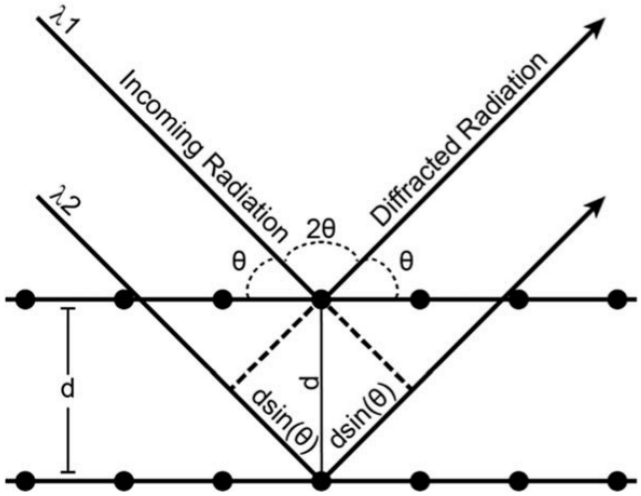

Figure 28: Schematic representation of the interaction between incident X-rays and a crystal lattice, used to obtain the Bragg's law (Stan C V et al. 2018)

Bragg's Law states that the symmetry and size of the unit cell determine the diffraction or position of the peaks, whereas the intensities of the peaks relate to the nature and positioning of atoms within the crystalline material's unit cell. The diffracted X-rays are then detected, processed, and counted. Due to the random orientation of the powdered material, all potential diffraction directions of the lattice should be acquired by scanning the sample through a range of 2θ angles. Because each compound has a unique set of d-spacings, converting the diffraction peaks to d-spacings allows identification of the compound. This is typically accomplished by comparing d-spacings to established reference patterns. XRD generates patterns of peak positions and relative intensities that represent various crystal structures and make it possible to detect their presence in unknown samples (quantitative analysis).

Quantitative phase analysis employs X-ray diffraction (XRD) patterns to determine the relative proportion of elemental components or phases. The intensity of the diffraction lines of a certain phase of a mixture is proportional to the amount of that phase in the mixture. Several quantitative approaches for mineral quantification based on XRD analyses have been proposed. In this study

the Rietveld method (Rietveld 1969) was used. In this method, using the least-square refinement (Bish 1993), each data point of an experimental diffractogram is compared to a calculated pattern.

$$R = \sum_i w_i \left| y_i(obs) - y_i(calc) \right|^2$$

where y_i(obs) and y_i(calc) are the observed and calculated intensities at point *i*, w_i is the weight assigned to each intensity, and y_i(calc) is the calculated intensity at each point (or 2θ step), which is obtained by summing contributions from the background and all neighboring Bragg reflections. Parameters such as preferential orientation, peak profile background, structure factor, cell parameters, scale factor displacement, are examined during the refinement process. XRD also provides information on how different hydrate phases are generated and can thus be used to determine the degree of hydration of anhydrous cement.

Sample preparation for XRD

The XRD patterns for the sample materials were done at the University of Padova using the X'Pert Pro diffractometer (PANalytical, Almelo, Netherlands) equipped with a Co-anode X-ray tube with generator settings of tension = 40 kV and current = 40 mA, Bragg-Brentano HD optical module, X'Celerator detector (with a detecting length of 2.12 2θ), time per step =99.6950 s and step size = 0.0170 2θ (Fig. 29).

Figure 29: X'Pert Pro diffractometer (PANalytical, Almelo, Netherlands)

The samples were ground to a fine powder (less than 5 μm) using a pestle and mortar. Very fine-grained powders are required for XRD analysis in order to minimize preferred orientation, produce a good signal-to-noise ratio, and avoid intensity fluctuations. Flat-plate reflection geometry (Bragg Brentano configuration) was used. To mount the sample onto the zero-background sample holder the back loading method was used (Fig. 30). The diffraction patterns were then analyzed using the software Profex (https://www.profex-xrd.org/) for quantitative analysis.


Figure 30: Backloaded XRD thesis samples

5.2 Thermogravimetric Analysis (TGA) and Differential Scanning Calorimetry (DSC)

Thermogravimetric analysis (TGA) determines the quantity and frequency of sample weight change against temperature and time in a controlled environment (Ng M H et al. 2018). When the temperature rises, the weight of the sample changes. The resulting curve is known as a thermogram, and each material has a unique thermogram due to the particular sequence of physicochemical reactions happening across certain temperature ranges and heating rates. TGA can be used to study the samples' thermal stability (the strength of the material at a particular temperature), oxidative stabilities (the rate of oxygen absorption on the material), and compositional qualities (Ng M H et al. 2018). Thermogravimetric analysis (TGA) is complemented by differential scanning calorimetry (DSC). Differential scanning calorimetry (DSC) is a technique that calculates the energy required to raise the temperature of a sample in comparison to a reference material. It provides quantitative and qualitative information on endothermic and exothermic processes occurring within the investigated temperature range.

The thermogravimetric analyzer is typically made up of a high-precision balance and a pan (usually platinum) which is then loaded with the sample. To precisely measure the temperature, the pan is placed in a small electrically heated oven equipped with a thermocouple which detects the temperature. To prevent oxidation or other undesirable reactions, the environment can be purged using inert gases (e.g., Argon). The analysis is carried out by progressively increasing the temperature and plotting weight against temperature.

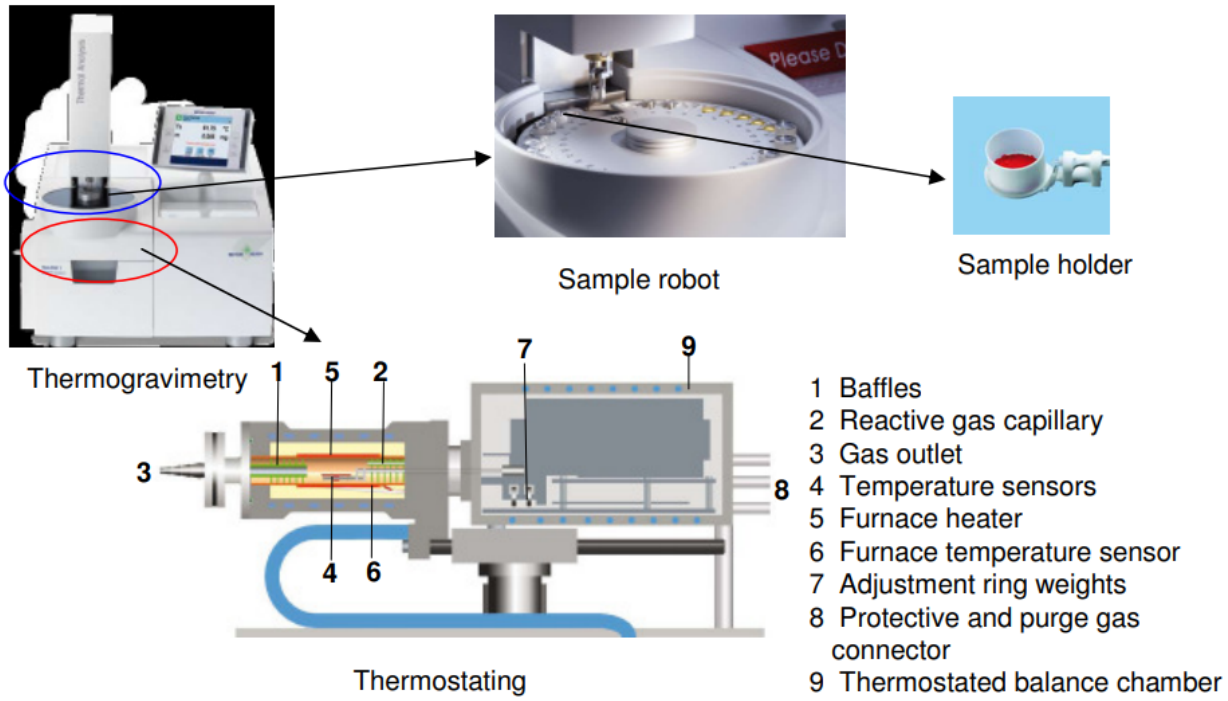

Figure 31: Thermogravimetric analyzer (EMPA)

Sample preparation for TGA

Finely ground samples (C, M1, M3, M4, M6, Q, S) were used for TGA/DSC analysis, which was carried out at the Department of Industrial Engineering. During the analysis, the temperature increased from 25˚C to 1000˚C at a rate of 10˚C/min (0.1667˚C/sec), this offered better resolution of the transitions than a higher temperature would. The TGA curves data were coupled with a derivative thermogram (DTG) curve to give a better resolution of the weight changes. The DTG curve was calculated from the TGA curve data by deriving the weight data as a function of temperature.

5.3 Scanning Electron Microscopy (SEM) and Energy Dispersive Spectroscopy (EDS)

Improving material efficiency demands a solid understanding of the material's composition, microstructure, and variability hence the use of techniques such as SEM and EDS. Scanning electron microscopy (SEM) is one of the most often utilized techniques for near-surface characterization of materials. It operates by scanning a finely focused electron beam across a surface and recording a variety of signals emitted by the electron-beam illuminated volume. SEM also permits the observation of elemental composition (e.g., by X-ray spectroscopy) and crystallographic nature (by backscattered electrons) of tiny volumes under the surface, in addition to observing the morphology of the surface of materials by recording secondary electrons (Zaefferer S et al. 2017). The SEM instrumentation is normally equipped with an EDS system

which allows the chemical analysis of features to be seen on the SEM display. Energy-dispersive X-ray spectroscopy (EDS) is a chemical characterization/elemental analysis technique for materials.

When using back scattered electrons (BSE), the image contrast is caused by the relationship between the mean atomic number and the backscatter coefficient. As a result, grey scale images are produced that can be utilized to distinguish phases and measure their proportion. Since the relevant phases in cement clinker have comparable mean atomic numbers, the technique cannot differentiate all phases. In comparison to BSE imaging, EDS mapping data can be used to improve the number of phases that can be detected. EDS data additionally provides information on minor and trace elements, which can be essential when identifying distinct cement clinker phases. EDS can detect major concentrations higher than 10 wt% and minor concentrations between 1 and 10 wt% though the detection limit would depend on the sample's surface conditions. A typical EDS spectrum is shown in Fig. 32.

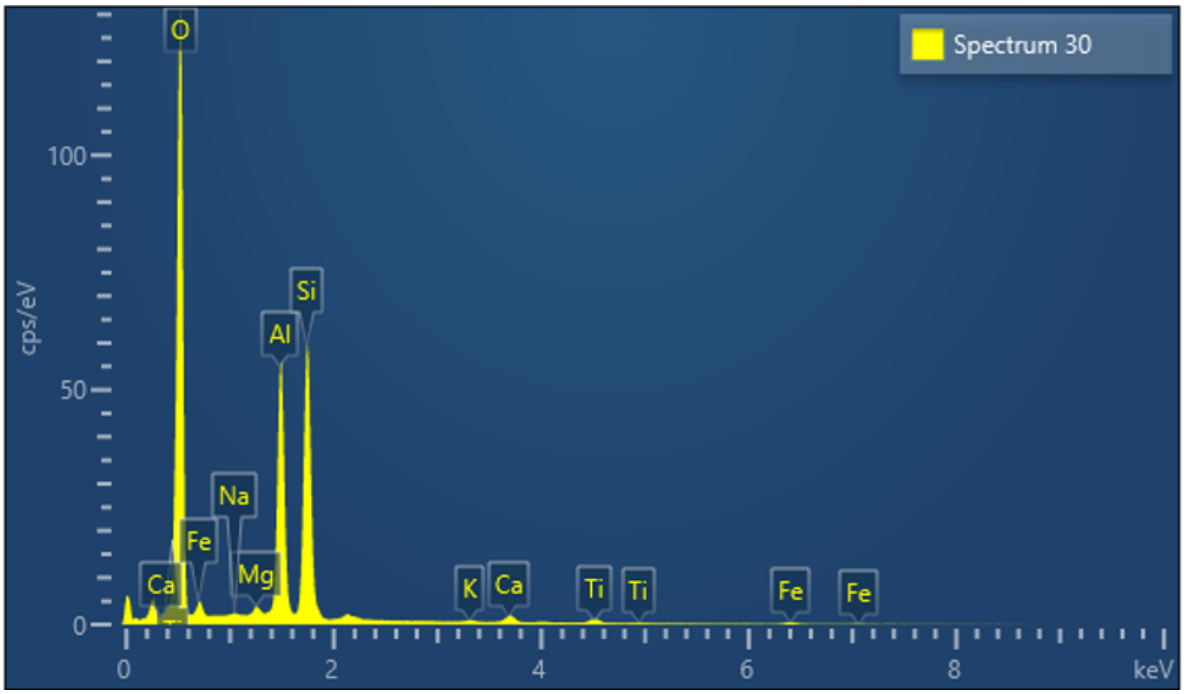

Figure 32: EDS spectrum of sample M1 used in this study

Sample preparation for Scanning electron microscopy (SEM)

For the SEM-EDS analysis, the samples were directly placed on sample holders using sticky tape. The experiment was carried out at the University of Padova using the Tescan Solaris scanning electron microscope shown in Fig. 33. The software package AZtec 5.0 (Oxford Instruments, UK) was used to acquire EDS data. The EDS spectra were quantified using the Oxford Instruments standard-less quantification algorithm, which can be found in the program AZtec 5.0 (Oxford Instruments, UK).

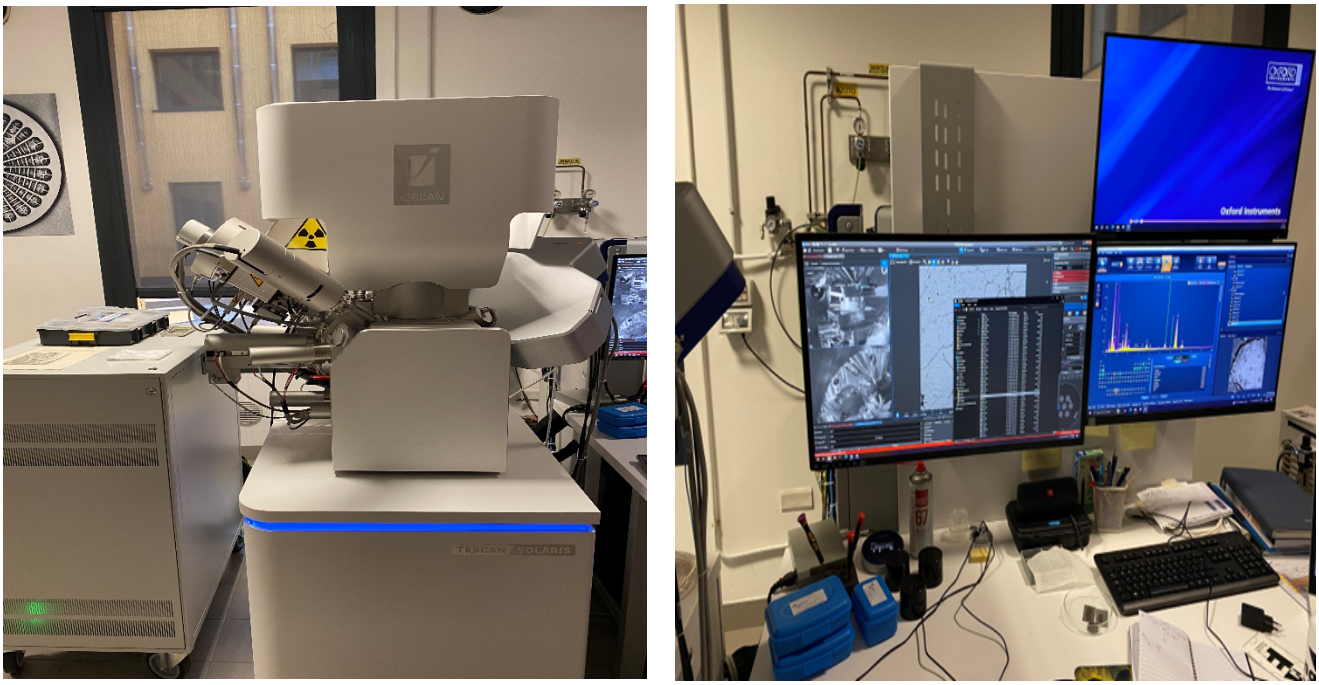

Figure 33: Tescan Solaris SEM and the Aztech software program at the University of Padova

5.4 Calorimetry

Calorimetry is the measure of heat and heat production rate during a chemical reaction. The most common applications of calorimetry in cement are kinetics and the study of cement hydration, by measuring the heat generated from the early hydration of cementitious materials. The timing and shape of temperature or heat curves acquired by calorimetry are indicators of the relative performance of cementitious mixes as well as potential interactions among the materials utilized in the mix. For cement and concrete applications, two types of calorimeters, isothermal and adiabatic calorimeters, have been used.

In isothermal calorimetry, the temperature is maintained constant. When cement paste hydrates and generates heat, the heat will flow from it and be measured as it passes through the sensor, such as a thermopile, towards the surrounding isothermal environment.

In adiabatic calorimetry, there is no heat exchange with the surrounding of the system. The chamber is entirely insulated, preventing heat flow in or out of it. Because complete insulation is impossible, a heating circuit and sensor are usually placed in the chamber to compensate for heat loss to the environment. If the addition of a heating circuit and sensor is not possible, numerical methods for predicting maximum temperature in mass concrete should be utilized.

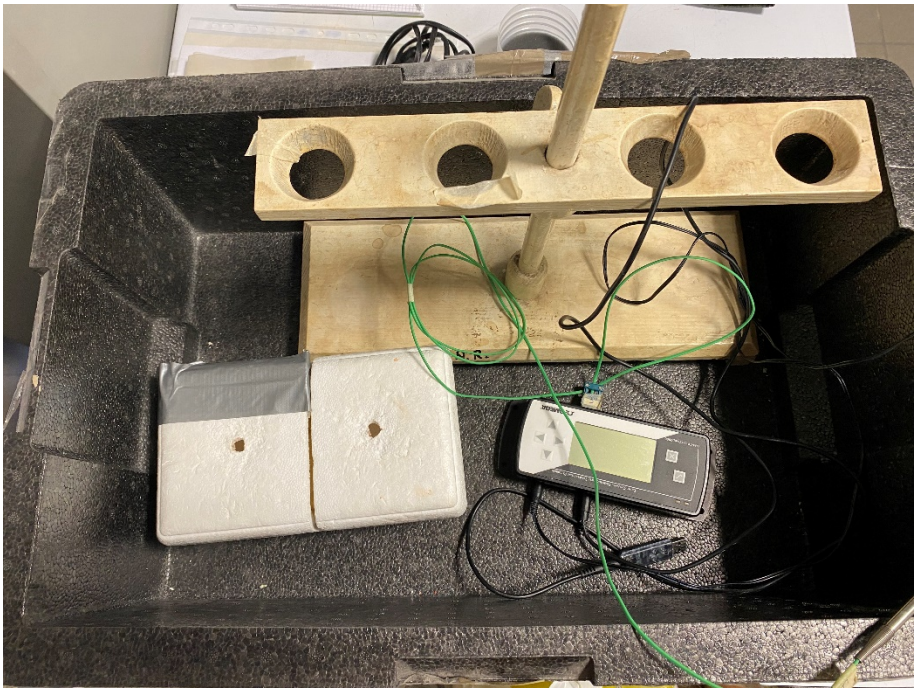

Figure 34: Calorimeter at the University of Padova

Sample preparation for Calorimetry

In this study "coffee cup" calorimetry was used, which is a semi-adiabatic method. A coffee cup calorimeter consists of a polystyrene (Styrofoam) cup with a lid. It is referred to as semi-adiabatic because, although it is very similar to adiabatic calorimetry in terms of insulation, no correction is being made on heat loss through insulator to the surrounding environment (Chung Chul Woo et al. 2016). Semi-adiabatic calorimetry tests were run on the two cement pastes named Sample 1 and Sample 2. All pastes had a water-to-cement ratio of 0.5. Before adding water, the dry components were combined and then water was added and mixed by hand for 2 minutes until a homogenous paste was achieved before pouring each paste into the coffee cups. The coffee cup was filled with a 50 % LC^3 + 50 % Soil and Quarry Dust blend and a thermocouple was inserted through the lid of the cup. The temperature increase inside the calorimeter was measured over 48 hours and was compared to that of the reference sample (50 % OPC + 50 % Soil and Quarry Dust blend).

5.5 Volume Strain

Volume changes in soils occur from the very beginning as the water content varies. In the initial hours and days, swelling occurs and after a certain period of time, shrinkage prevails.

Sample preparation for volume stability experiments

Both soil- quarry dust blends with LC^3 and OPC were measured to quantify their volumetric changes. The mixtures consisted of 9.5 g Clay, 0.5 g cement (OPC or LC^3) and 3g water. Before adding water, the mixture was blended and then, upon addition of water, stirred for 1 minute with a mixer to obtain a homogeneous paste. The pastes were then placed in a cylindrical plastic container to mold them, then kept at 95% relative humidity for 48 hours. After 48 hours, the molds were removed, and the length of each sample was measured using calipers. Subsequently, digital length comparators were used to measure the length variation in time, for a period of two weeks.

CHAPTER 6 - RESULTS

The results from this study will be discussed in this chapter.

6.1 XRD

Six samples (C, Q, S1, M1, M3, M4, M6) were analyzed using XRD to understand their compositions with results shown in Fig. 35-42. The phases present in the samples are also shown in Table 8. The raw materials C (Clay), Q (Quarry dust), and S1 (Limestone calcined clay cement) were analyzed first, followed by the soil-quarry dust combinations (M3, M4, and M6) to understand their reactions with cement. The C sample largely consists of kaolinite (85.8%) and lower contents of non-clay phases such as goethite, illite and quartz.

In the S1 sample C_3S is shown to have the strongest peaks as it is the highest phase in quantity (C_3S is the most abundant clinker phase in cement). Additionally, adequate amounts of gypsum and belite are present in S1, contributing to the final strength of the cement. Since LC^3 is a composite cement with a significant amount of calcined clay and limestone, several phases typical of clay soils (e.g., feldspars, hematite, quartz) as well as calcite from the limestone fraction were identified.

Aluminous zeolites such as phillipsite and analcime were detected in the quarry dust (Q) sample, these zeolites usually form from the alteration of basic glasses. Phillipsite is typically formed in K-rich volcaniclastics such as tuff deposits, the quarry dust was obtained from a tuff deposit in Meru, Kenya. Analcime is a Na-rich zeolite formed through the reaction of volcanic glass or zeolite precursors with Na-rich fluids, its peak has higher intensity than those of the other phases suggesting that it is higher in quantity. The other phases found in the sample are feldspar, plagioclase which could be dominant minerals of the mineralogy of the area. The phase rutile is very low in composition (0.8%)

Samples M1, M3, M4 and M6 are largely dominated by kaolinite as they consist of 60% of neat clay soil (C) which is primarily composed of kaolinite. They also contain feldspar, plagioclase, albite, phillipsite and analcime in moderate amounts and lower contents of anatase, gypsum quartz and goethite. The quartz observed in the M1, M3, M4 and M6 samples is derived from the calcined clay. The samples also contain small amounts of the reaction products ettringite and hemicarboaluminate (M1 and M3) from the reaction of calcium carbonate from limestone with alumina phases from the soil in samples M1 and M3. The low content of the reaction products is due to the small dosage of cement (1% and 5%).

Table 8: XRD results of the samples.

Mineral Phase	C	Q	S1	M1	M3	M4	M6
Quartz	X		X	X	X	X	X
Kaolinite	X			X	X	X	X
Goethite	X			X	X	X	X
Chlorite ----	X						
Analcime		X		X	X	X	X
Rutile		X	X				
Phillipsite		X		X	X	X	X
Feldspar		X	X	X	X	X	X
Portlandite			X				X
Gypsum			X	X	X	X	X
Calcite			X				
Plagioclase		X		X	X	X	X
Hematite			X				
Anatase	X			X	X		X
Ettringite				X	X	X	X
Hemicarboaluminate				X	X		
Clinker Phases							
Aluminate (C_3A)			X				
Alite (C_3S)			X				
Belite (C_2S)			X				
Ferrite (C_4AF)			X				

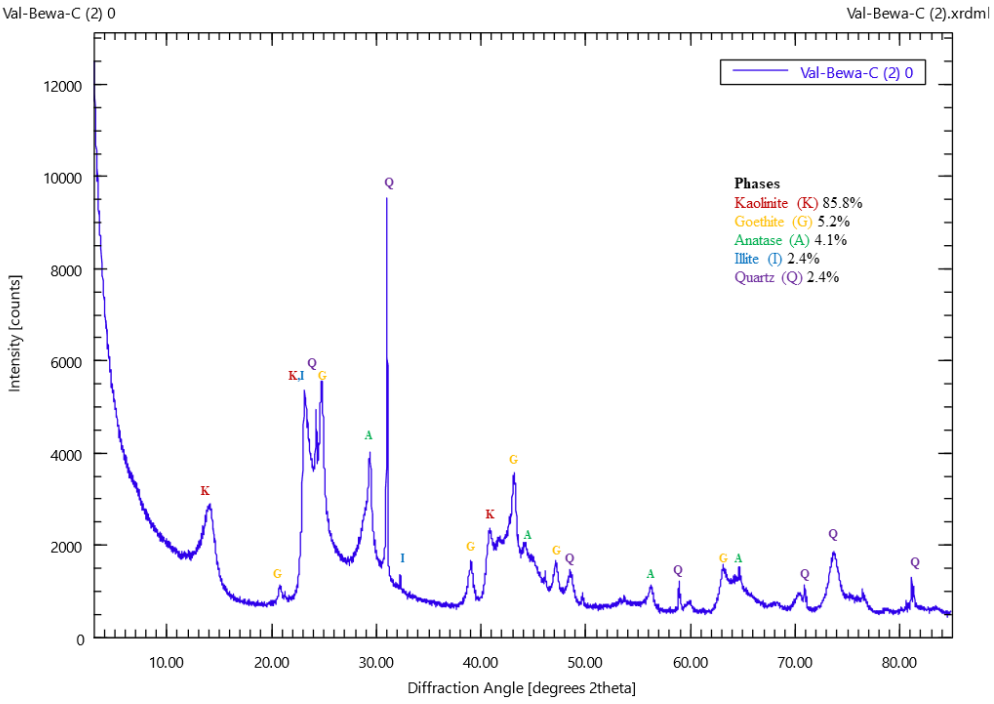

Figure 35: XRD of the C sample

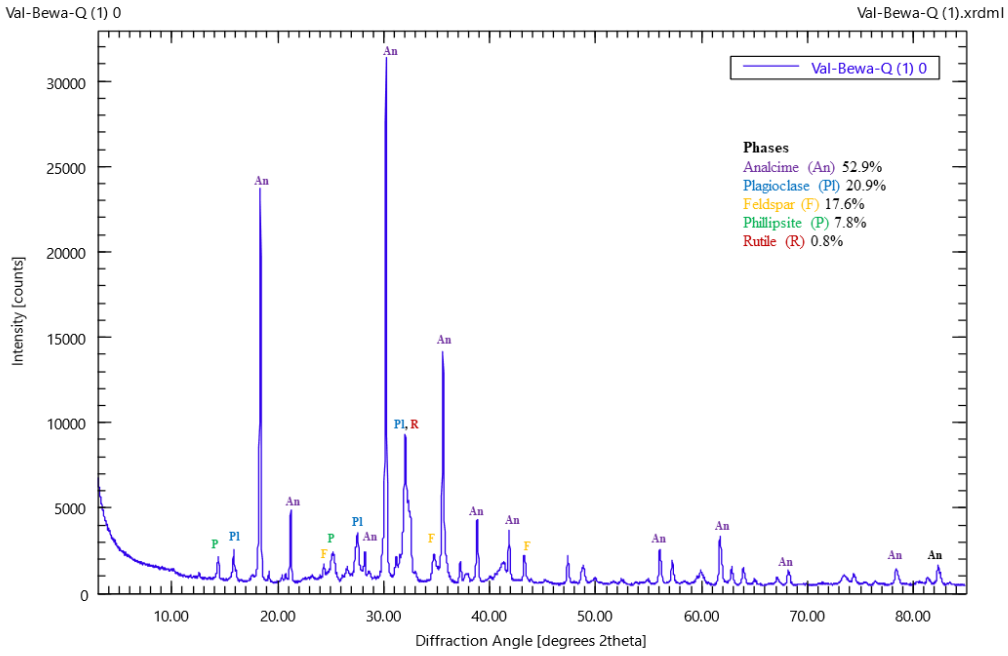

Figure 36: XRD of the Q sample

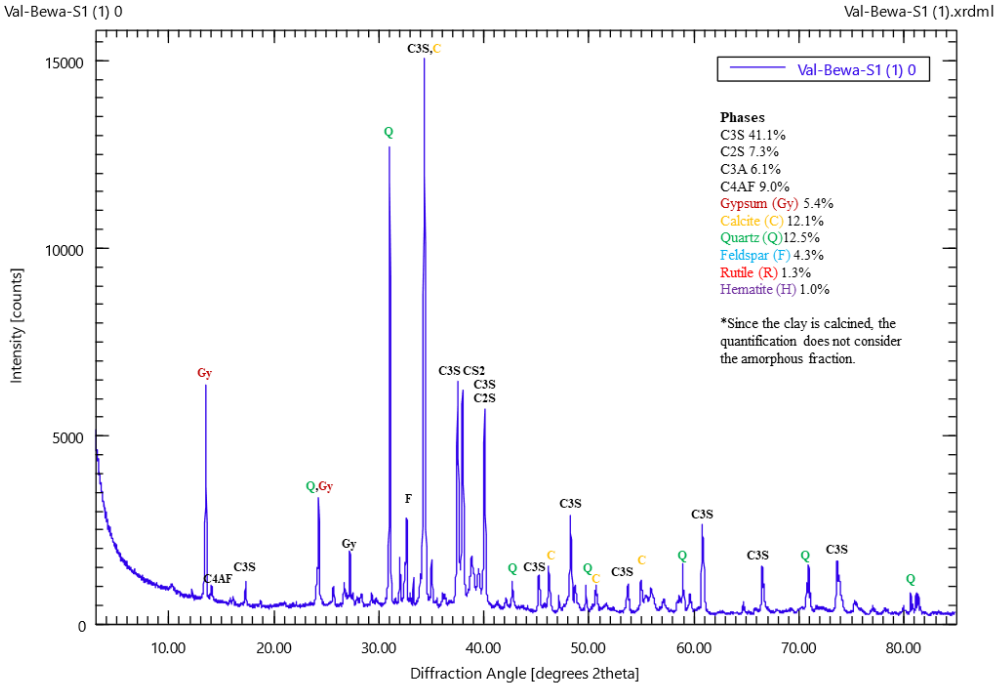

Figure 37: XRD of the S1 sample

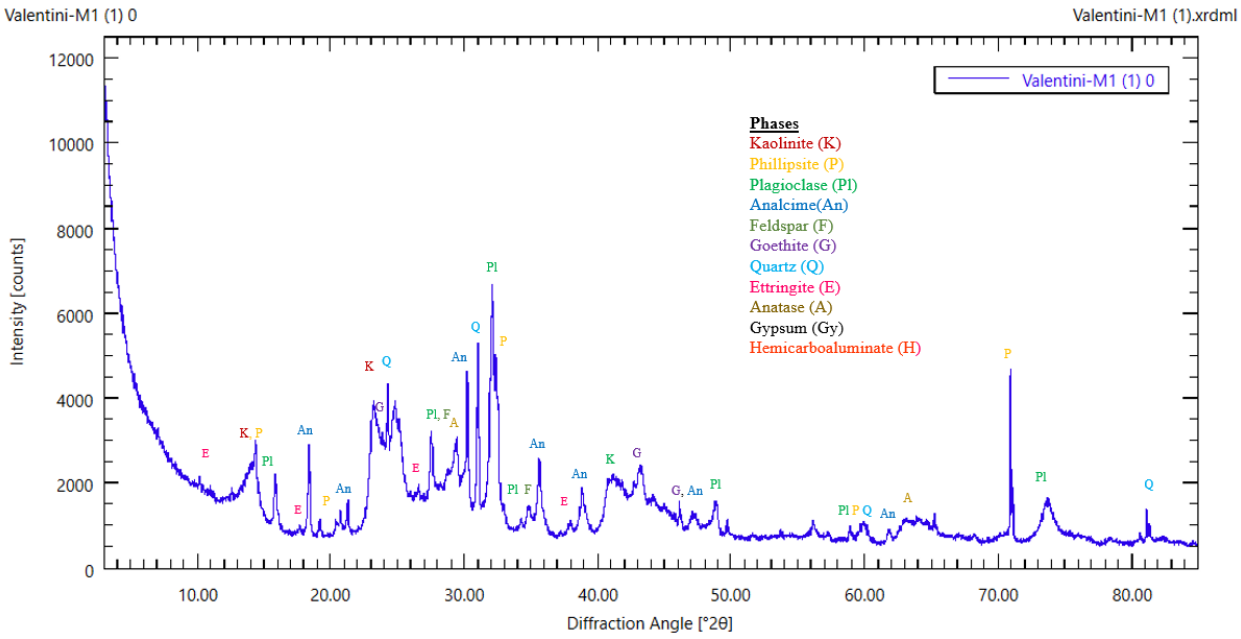

Figure 38: XRD of the M1 sample

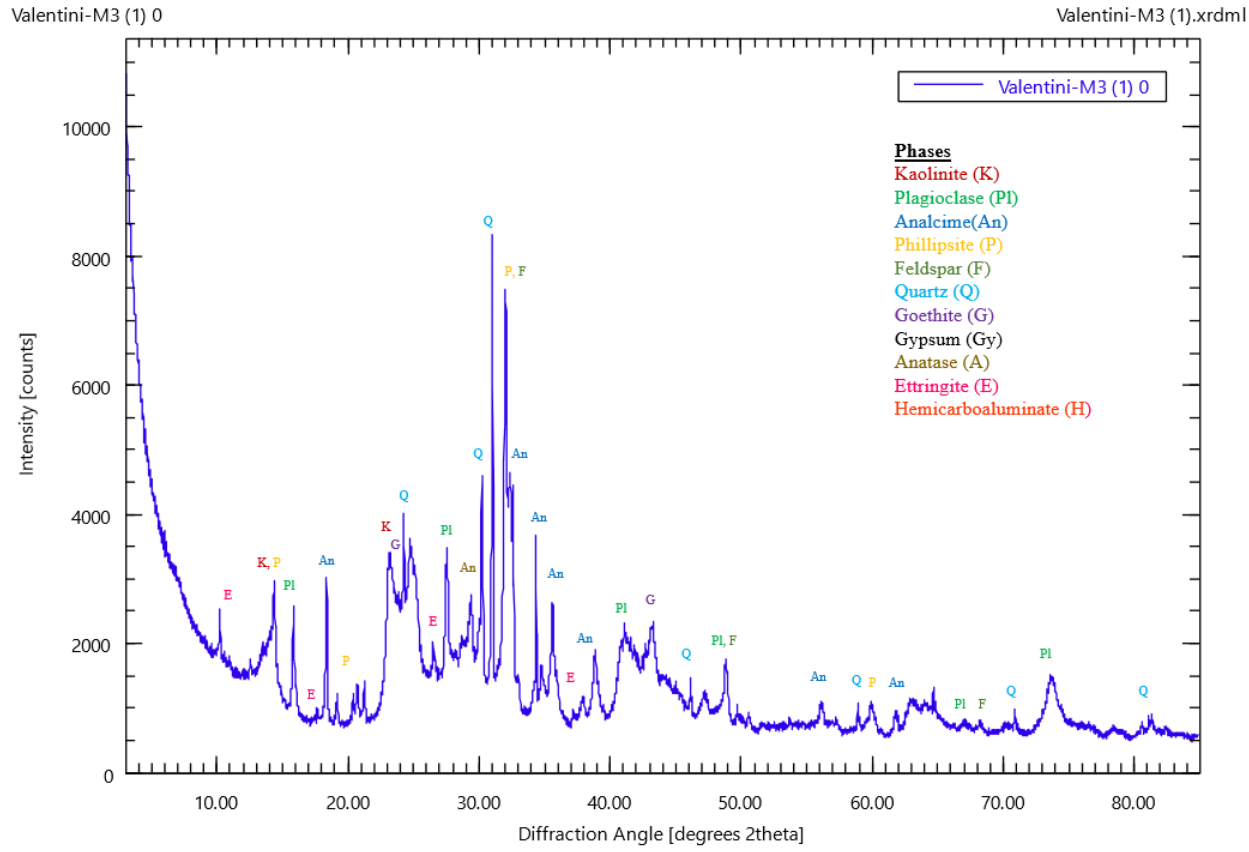

Figure 40: XRD of the M3 sample

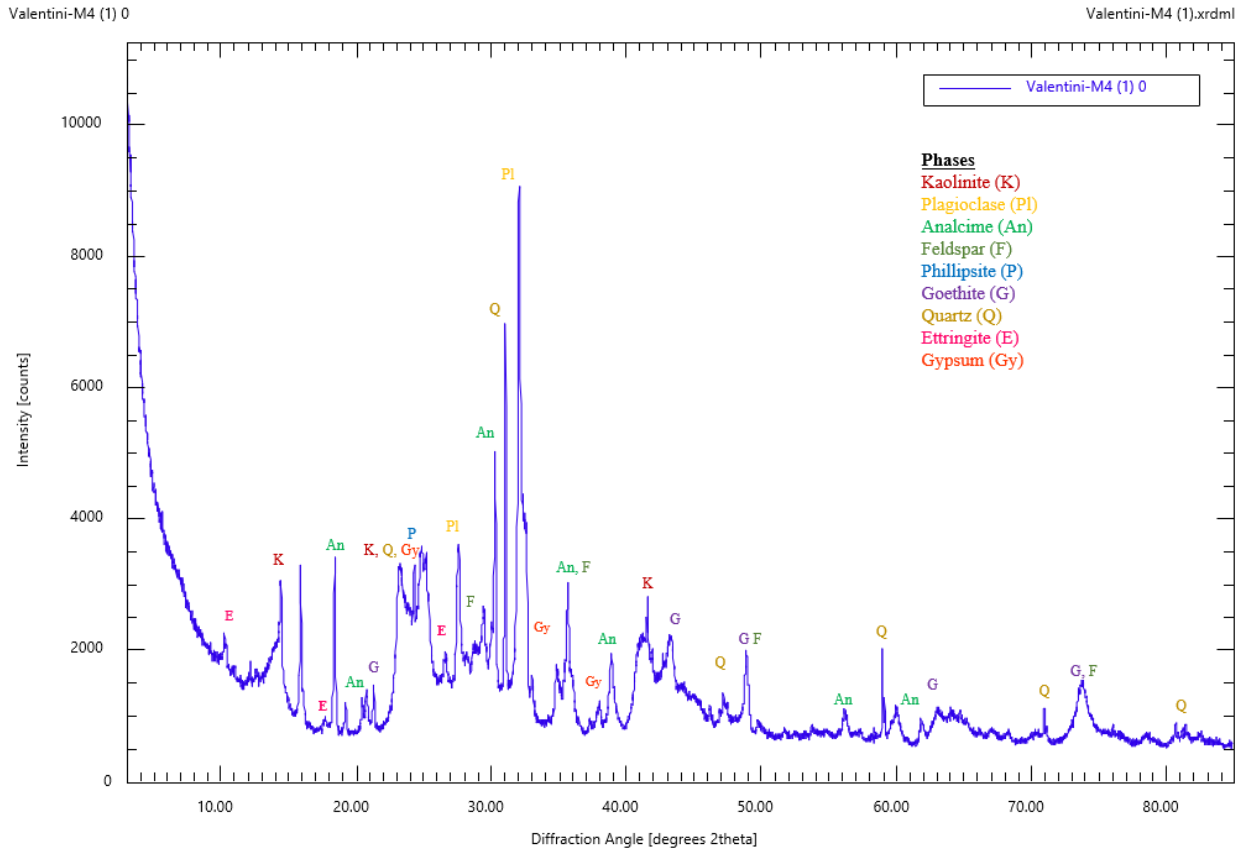

Figure 41: XRD of the M4 sample

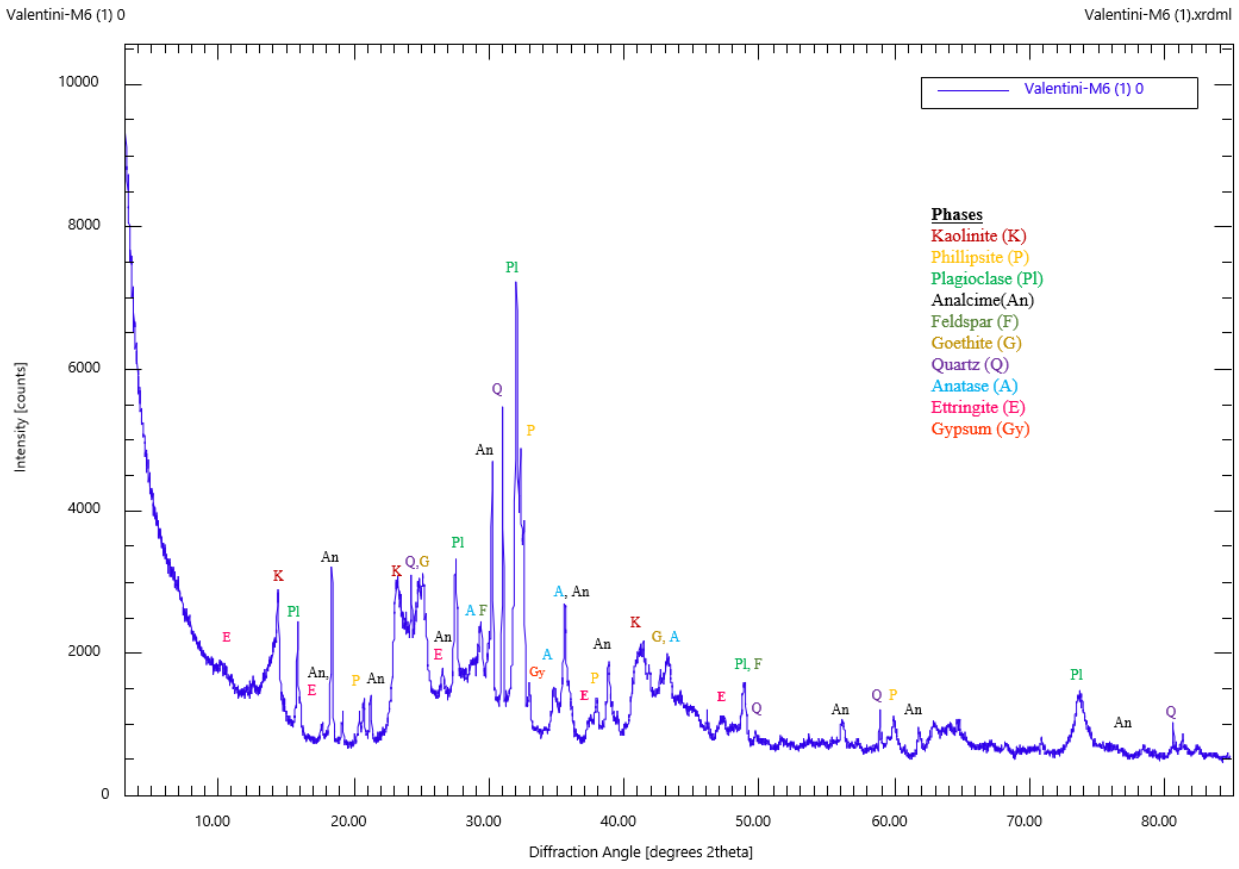

Figure 42: XRD of the M6 sample

6.2 Scanning Electron Microscopy (SEM) and Energy Dispersive Spectroscopy (EDS)

SEM-EDS analysis on paste samples was utilized to examine the microstructure of neat clay sample (C), and the soil-quarry dust cement mixtures M1 and M6 used in this study, as shown in Fig. 43. The SEM analysis of the clay sample (C) reveals loose aggregates as the sample is distabilized whereas in both the M3 and M6 samples aggregates are more compact as the samples are stabilized. The M6 sample is more compact than the M3 sample, which can be ascribed to a better development of a hydrated cement matrix that acts as a binder and holds the soil particles together. Both the M3 and M6 samples show some smooth cavities as shown in Fig. 44, which can be associated with the composition of the quarry dust, which is compatible with a volcanic tuff. Tuff rocks typically display cavities, formed by volcanic degassing.

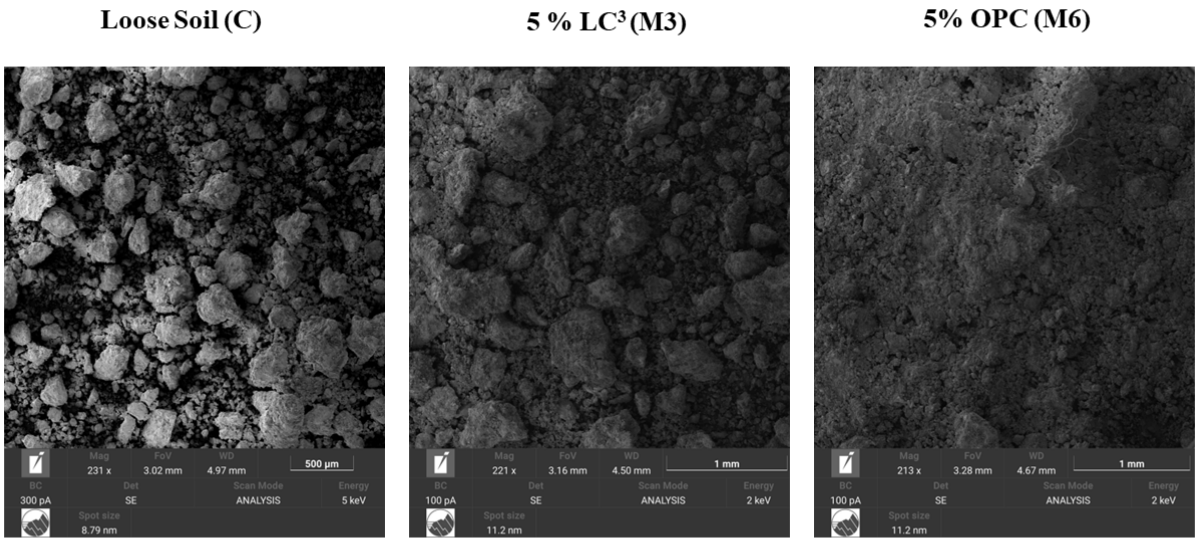

Figure 43: SEM analysis for samples C, M3 and M6

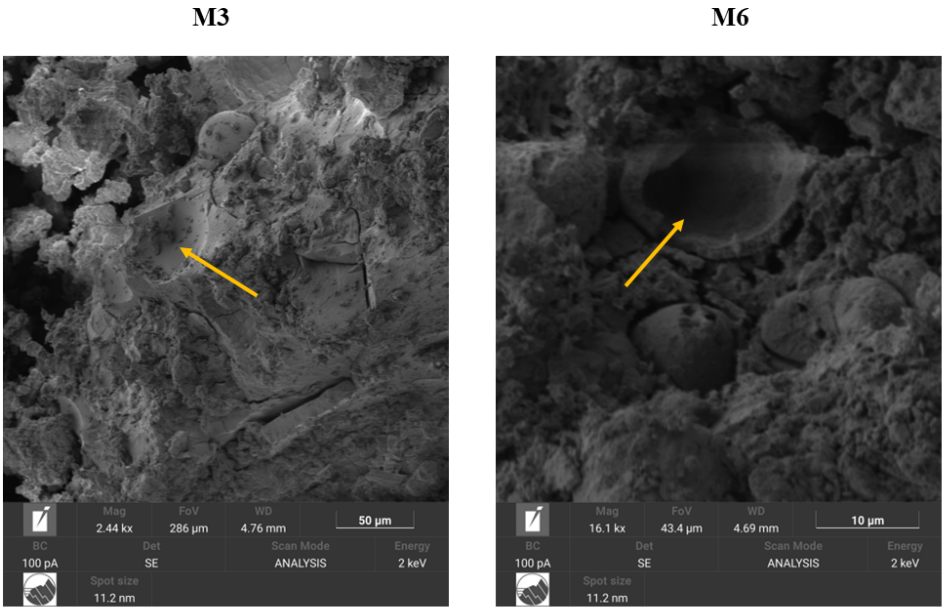

Figure 44: Cavities in samples M3 and M6 shown by the arrows

In all the samples, the chemical analysis performed by EDS shows the predominance of Si, Al and O peaks. Traces of iron (Fe), calcium (Ca) and potassium (K) are also found in the mineral phases of samples M3 and M6. Small peaks of titanium (Ti) are present in all the samples indicating that it is present in trace amounts. The predominant chemistry in the samples is that of soil and quarry dust as these mixtures contain only up to 5% hydrated cement. The EDS spectrums of the C, M3 and M6 samples are also in agreement with their XRD results and mineralogy as they contain high peaks of silica, aluminum and oxygen, minor peaks of calcium and magnesium and trace amounts of titanium which are the mineral constituents of the phases found.

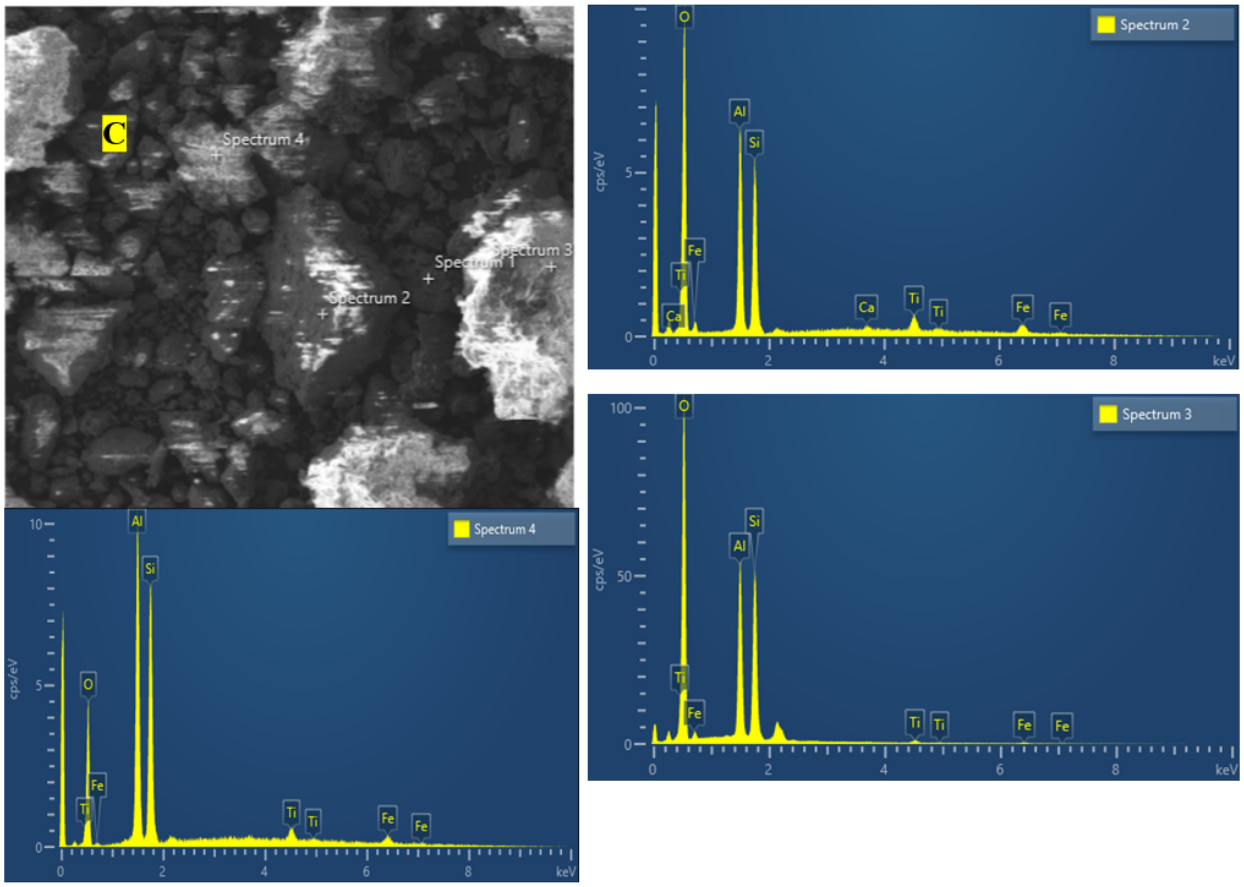

Figure 45: EDS of sample C

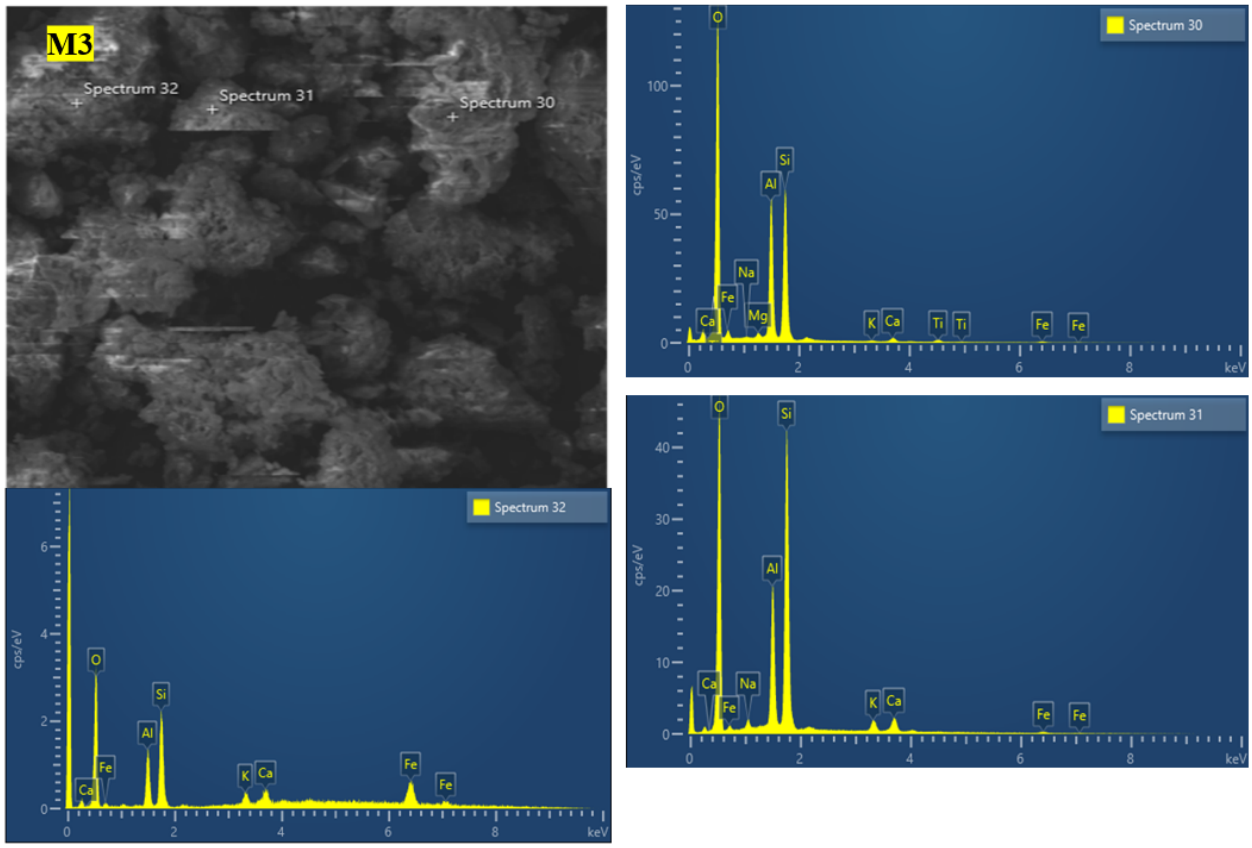

Figure 46: EDS of sample M3

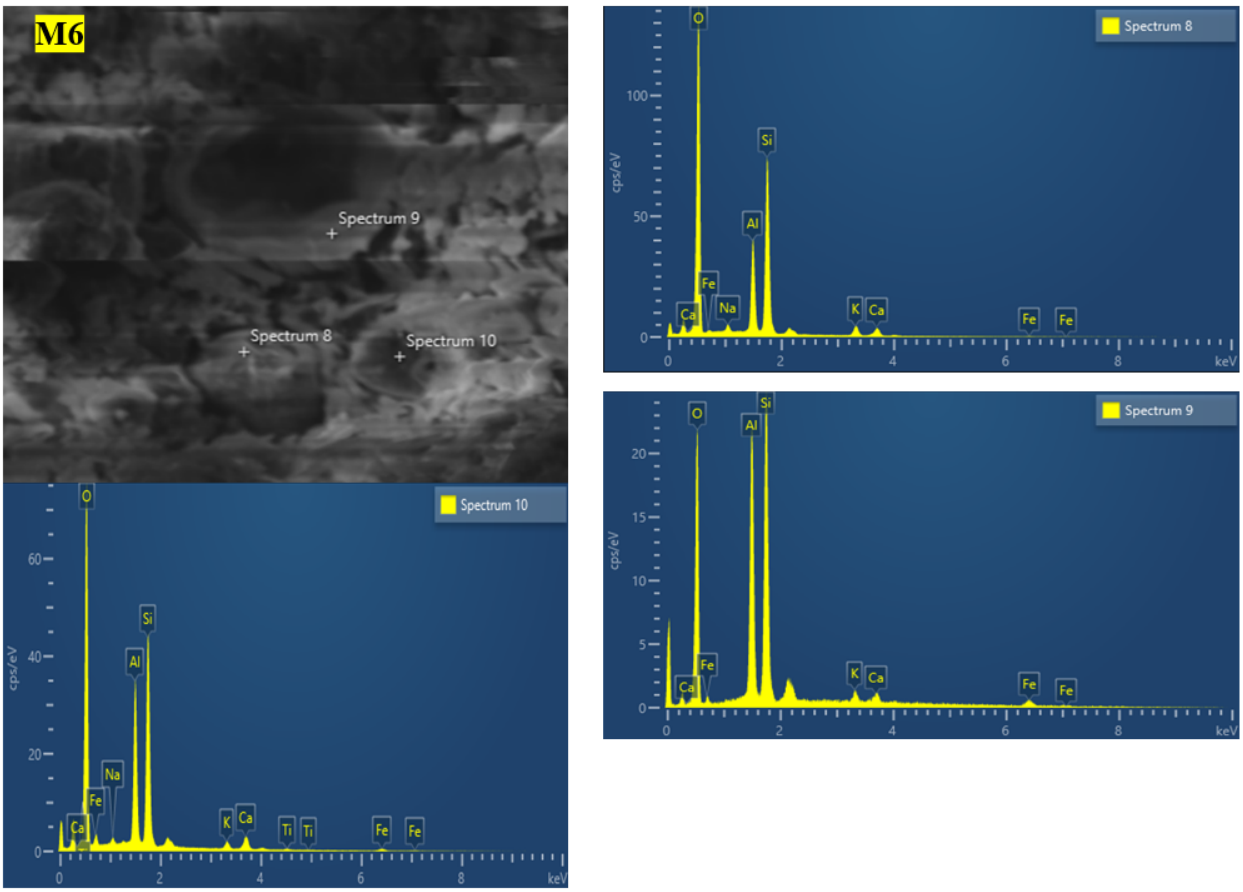

Figure 47: EDS of sample M6

6.3 Thermogravimetric analysis (TGA)

TGA was performed for all the samples to quantify the weight changes due to thermal decomposition. Derivative thermogravimetry was also calculated to allow a better resolution of the consecutive weight changes. The resultant graphs are shown in Fig. 48-54. In the clay sample (C), between 80 to 150˚C there is the release of free or sorbed water which leads to a huge amount of weight loss as shown in the TGA plot. This dehydration is endothermic as shown in the DSC plot. This is followed by the combustion of organic matter between 200 and 350˚C which is an exothermic reaction. At about 400 ˚C, there is a mass loss due to endothermic dihydroxylation where there is the loss of bound water or the dissociation of hydroxyls from the lattice which may cause amorphization of the lattice structure of kaolinite.

When temperature rises above 20˚C, cementitious materials undergo a series of complex physical and chemical changes. The TGA result of the LC^3 (S1) sample is shown in Fig. 49. In the TGA graph, the near flat curves between 150 to 650 ˚C suggested metakaolin had replaced the kaolinites in the clay during the calcination process. As can be seen from the XRD graphs the calcined clay sample (Fig. 35) does not contain kaolinite. As the temperature increases from 20˚C to 300˚C,

evaporable water is released and escapes the samples leading the calcium aluminate hydrate (C A) S H) phases to become dehydrated and hence mass loss. Endothermic peaks are seen for ettringite (AFt), monocarboaluminate, hemicarboaluminate, and monosulfate which all lose water at approximately 100˚C, 170˚C, and 190˚C, respectively (Weerdt De K et al. 2010). The dehydration of portlandite (CH) takes place between 400 and 500˚C as shown in the DTG graphs (Fig. 49), this resulted in an endothermic peak in the DSC graph. Additionally, the decomposition of calcite and release of carbon dioxide to generate calcium oxide between 600 and 800˚C is what causes the weight loss in that range. The amount of limestone added influences how much weight is lost in this temperature range.

In the samples M1, M3, M4 and M6, the mass loss is mainly due to dehydration, combustion of organic matter and dihydroxylation of the clay as the samples are primarily composed of clay and just 1-5% cement. Some of the weight lost in the samples containing quarry dust (Q, M1, M3, M4 and M6) could be attributed to the presence of the zeolites, analcime and phillipsite as shown by the XRD of the quarry dust sample (Q). According to Sandoval et al (2009), analcime has three well defined dehydration steps at 140, 415 and 980 °C. In the DTG analysis of samples Q, M1, M3, M4 and M6, a dehydration step can be seen at 140°C which could be attributed to the loss of crystalline water from analcime. Phillipsite loses water in the temperature intervals 100-400°C and 400 to 695°C (Rykl D et al 1991). The mass loss in these ranges for our samples could additionally be due to the dehydration of phillipsite. The loss of crystalline water from phillipsite is however greater in the temperature range 100-400°C, hence the higher weight loss in that range.

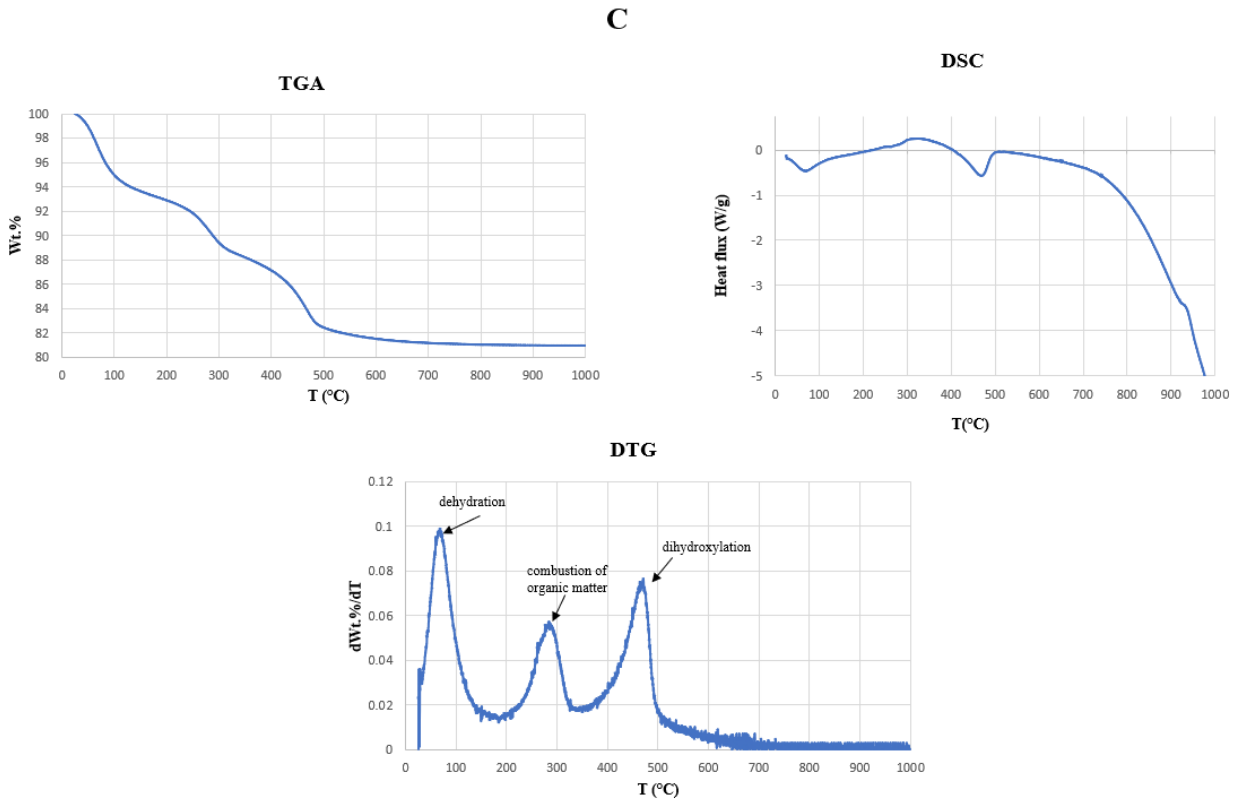

Figure 48: TGA, DTG and DSC plot for sample C

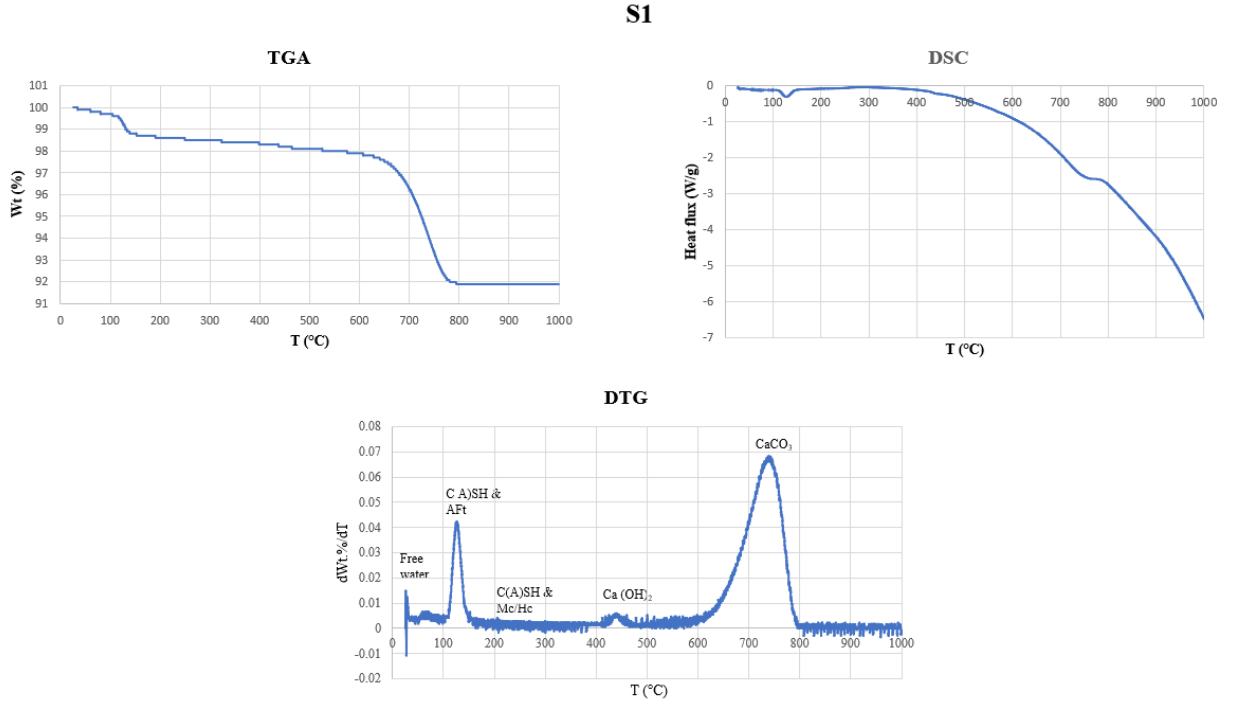

Figure 49: TGA, DTG and DSC plot for sample S1

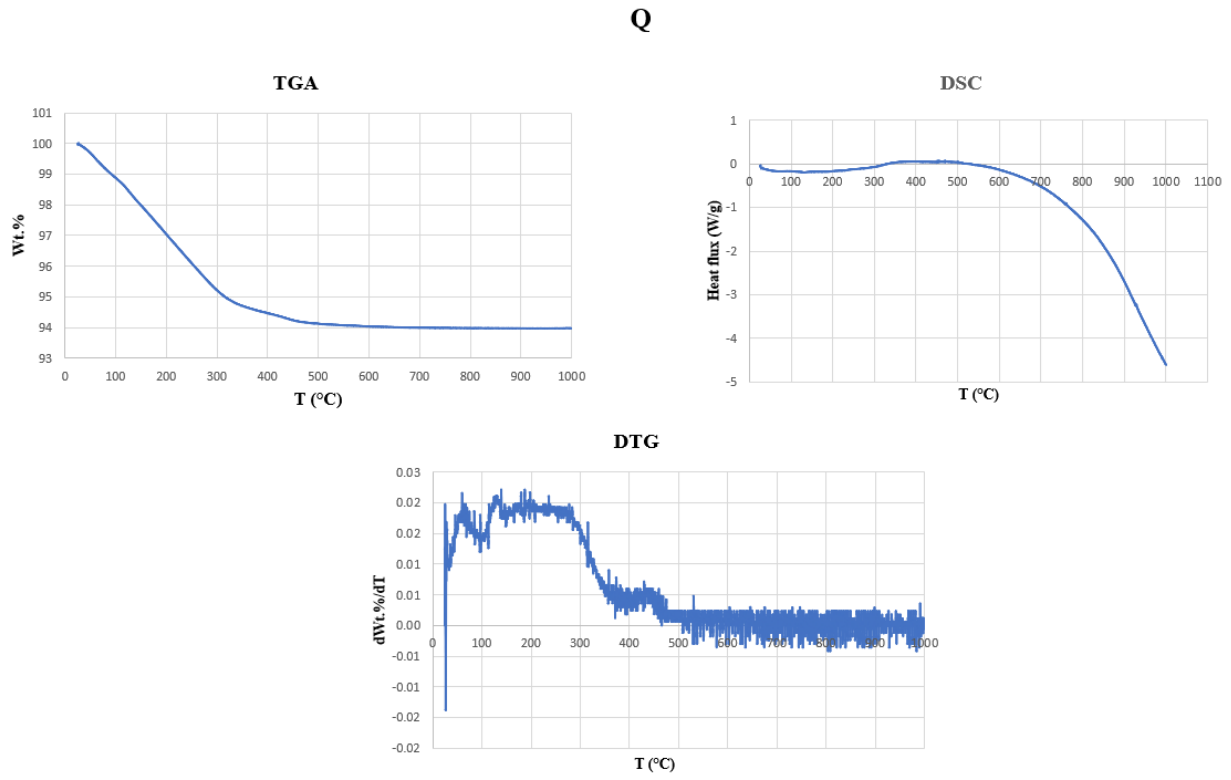

Figure 50: TGA, DTG and DSC plot for sample Q

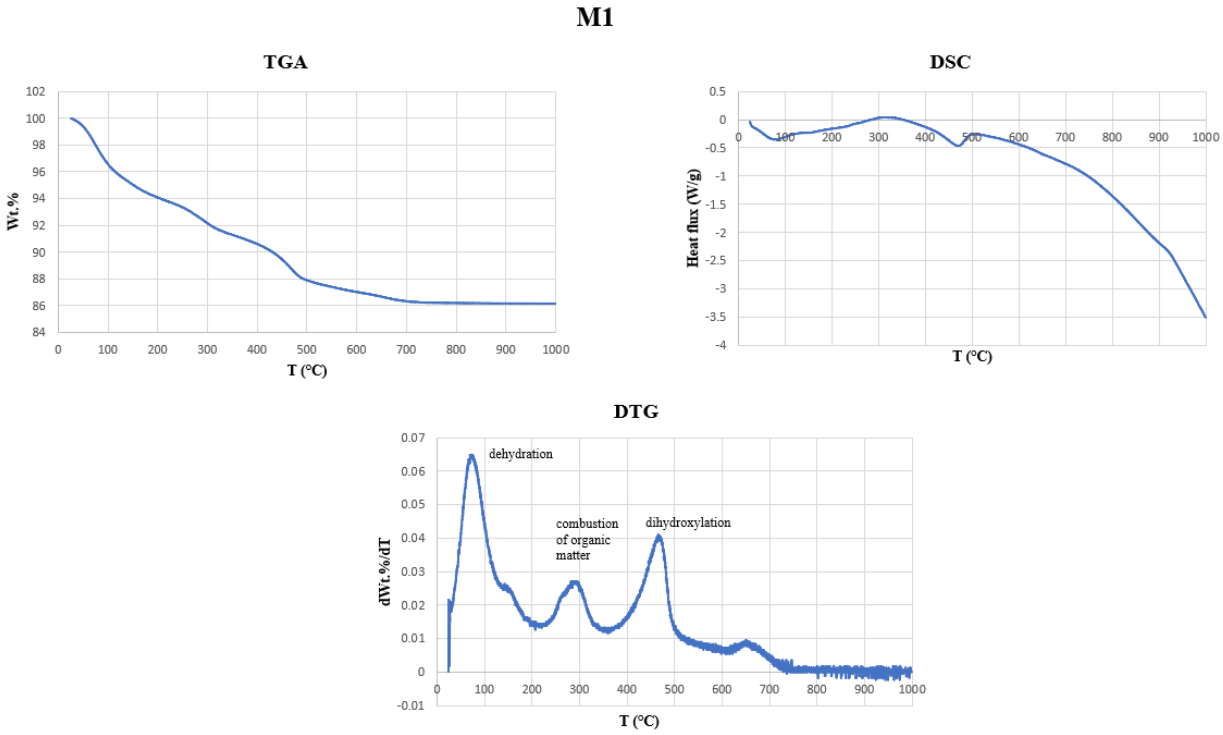

Figure 51: DTG and DSC plot for sample M1 showing the dehydration, combustion of organic matter and dihydroxylation of kaolinite

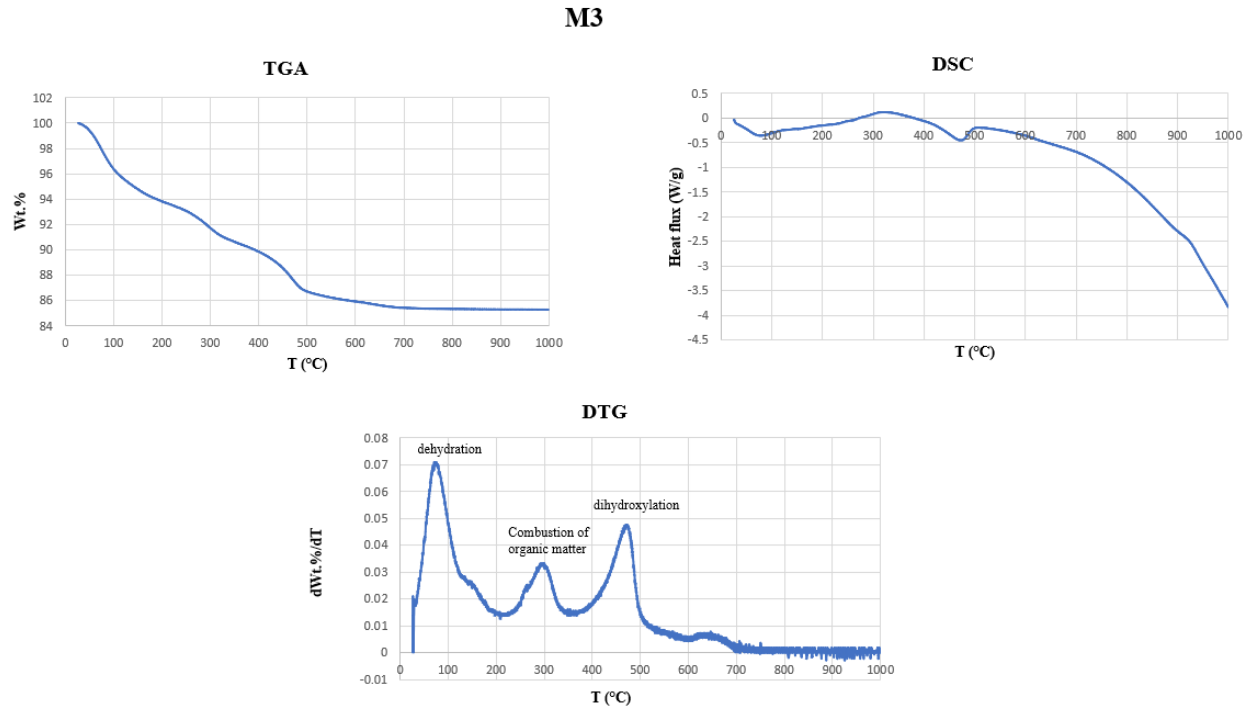

Figure 52: TGA, DTG and DSC plot for sample M3 showing the dehydration, combustion of organic matter and dihydroxylation of kaolinite

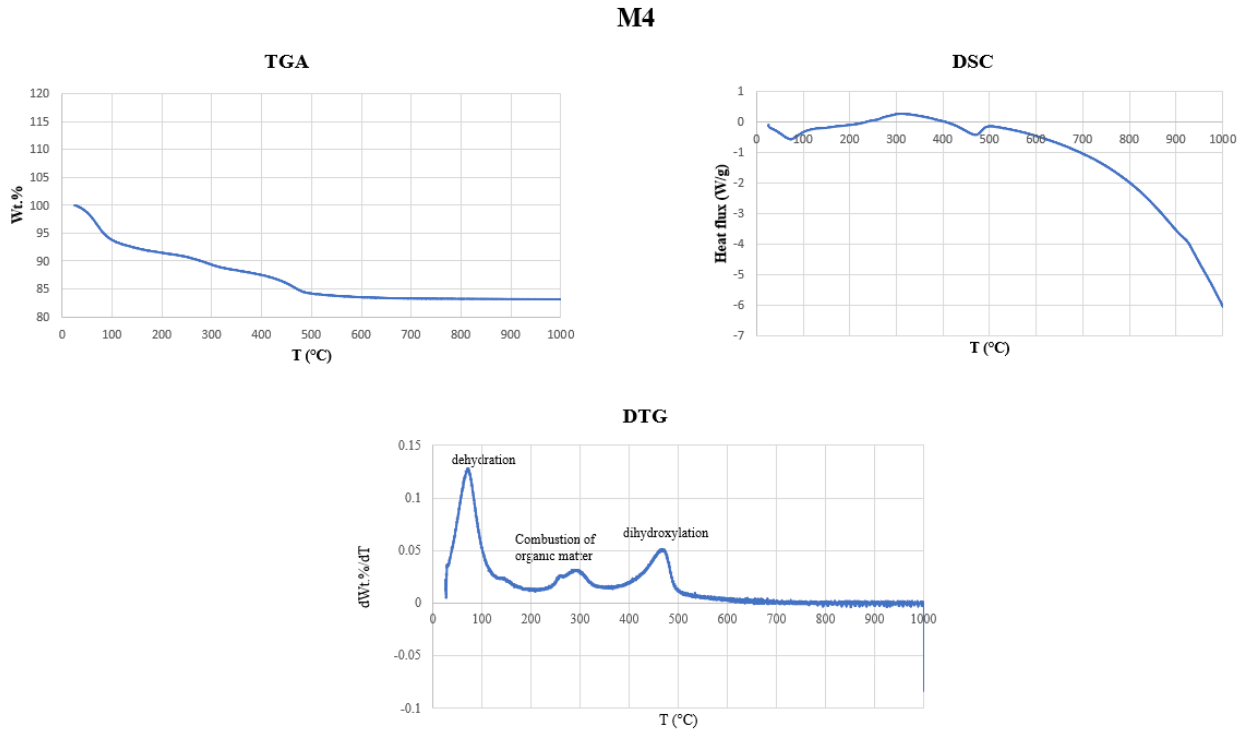

Figure 53: TGA, DTG and DSC plot for sample M4 showing the dehydration, combustion of organic matter and dihydroxylation of kaolinite

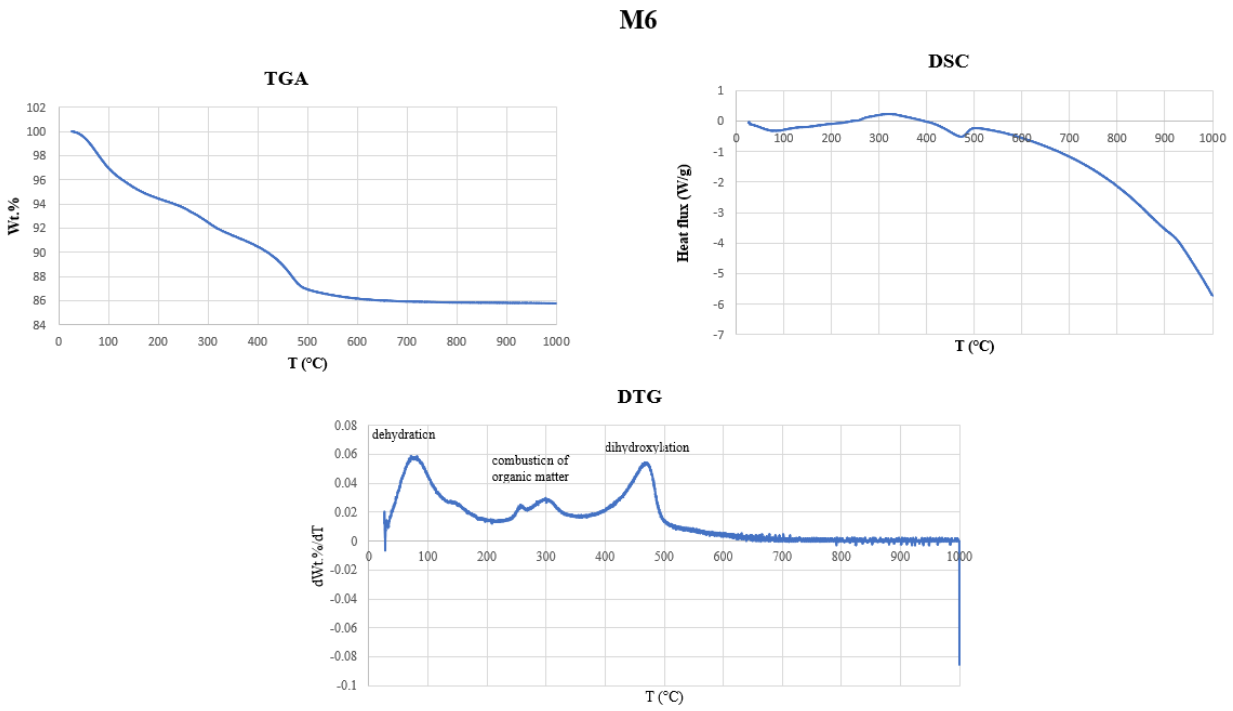

Figure 54: TGA, DTG and DSC plot for sample M6 showing the dehydration, combustion of organic matter and dihydroxylation of kaolinite

6.4 Volume Strain Analysis

The volumetric changes of soil-quarry dust mixes with LC^3 and OPC were quantified using digital length comparators over a period of two weeks. The LC^3 mix sample was compared to the OPC mix sample as a reference and the results are shown in Table 9. The LC^3 mix sample exhibits a higher volume change compared to the mixture with OPC. The loss of moisture from the soil appears to be the cause of shrinkage. As shown by the XRD, the samples contain a large amount of kaolinite which is prone to expansion and shrinkage through absorption and desorption of water. The SEM results also indicate that LC^3 has a less efficient stabilizing power to OPC hence its higher volume change.

Table 9: Results for the volume strain analysis

Initial Length LC3 (mm)	Initial Length OPC (mm)	Time (days)	Variation LC3	Variation OPC	Volume Strain LC3	Volume Strain OPC
8.4	13	7	-0.538	-0.391	-0.0640	-0.0301
		14	-0.542	-0.395	-0.0645	-0.0417

6.5 Calorimetry

Fig. 55 shows the calorimetry curves for LC^3 and OPC. This is a typical calorimetry curve for cements in which we see a first peak associated with the rapid initial dissolution of C_3S and the release of Ca^{2+} and OH^- ions into solution during the initial phase. Since the solution is still considerably undersaturated in terms of C_3S, dissolution proceeds rapidly leading to the etch pitting of C_3S surfaces. This peak is associated with a maximum in the rate of heat evolution. This stage was followed by the dormant period, which is a period of low reactivity brought by the dissolution control due to etch pit coalescence and slow precipitation of C-S-H. The second and main peak of the heat of hydration is associated with C_3S dissolution, C-S-H and portlandite precipitation occurs, this stage marks the acceleration period. The deceleration period is due to the lack of a reactive surface area resulting in a gradual decrease in the rate of hydration. In the last stage, the rate of reaction decreases continuously due to a congested microstructure of C_3S that is covered by C-S-H particles. Any further reaction would be controlled by the nano pores of the C-S-H particles hence the retardation of the reaction.

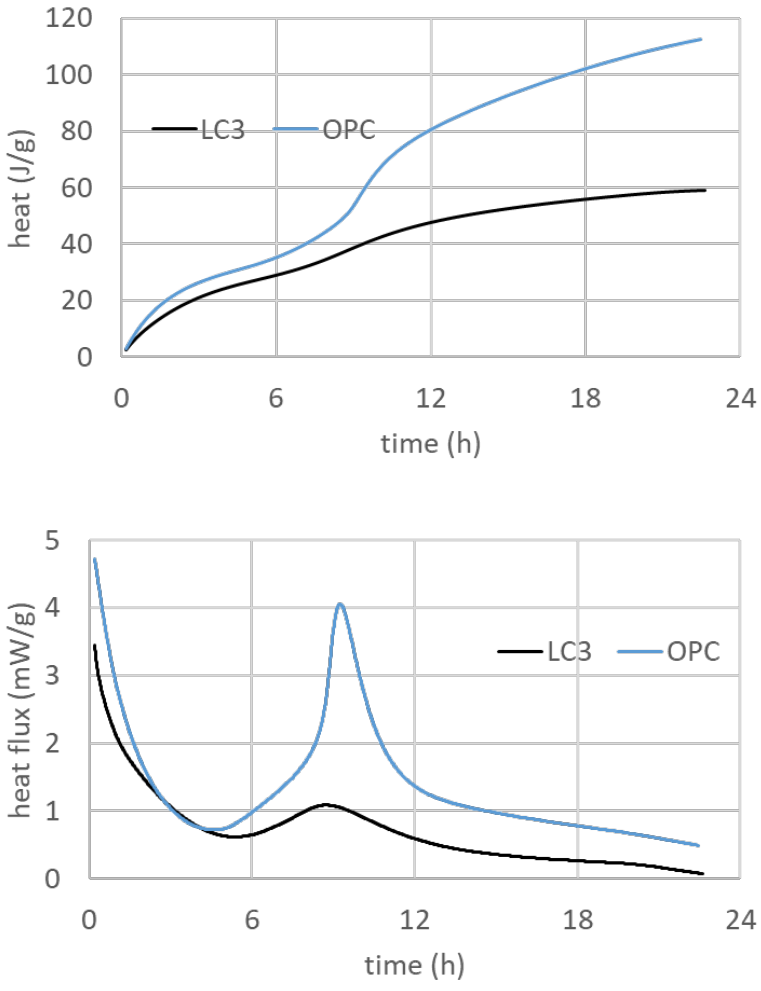

Figure 55: Isothermal calorimetry curves for OPC and LC^3

CHAPTER 7 - DISCUSSION

For measuring the phase composition of multicomponent materials such as OPC and LC^3, complimentary characterization methods such as XRD and SEM and EDS were used to obtain a better picture of both OPC and LC^3 phase compositions. From the XRD analysis, the kaolinite content of the clay sample is 85.8% percent. The preliminary analysis identified the soil used in this study to be highly plastic (Table 5). Since the XRD analysis shows that the soil is mainly composed of kaolinite, it cannot be classified as an expandible clay as there are no smectites. The structure of kaolinite is formed by two sheets with two distinct layers which are linked by hydrogen bonding involving alumina (AL-OH) and siloxane (Si-O) groups, these bonding forces mean that kaolinite is a non-expandible clay. This soil can, however, be classified as a plastic kaolin because of the expansion and shrinkage that may occur due to the absorption or desorption of water. According to Christidis E G (2011)'s chart for identifying clays based on their plasticity index (PI), the PI of this clay according to the preliminary analysis (Table 5) fell within the range of a plastic kaolin. The plasticity is thus associated with the large amount of kaolinite.

The clay sample (C) exhibits loose aggregates as there is no binder in it. Both the M3 (5% LC^3) and M6 (5% OPC) show a compact matrix indicating that C-S-H has formed and hence stabilization. C-S-H enhances the cementitious qualities of the cements' paste thus increasing its strength and stability. The M3 and M6 samples both contain 40% quarry dust, their XRD analysis are shown in Fig. 40 and 42. The amorphous silica present in the quarry dust may possibly react with the calcium hydrates (CH) formed during cement hydration, which produces additional cementitious components like C-S-H gel. The XRD analysis of quarry dust Fig. 36 shows the presence of the zeolites, analcime and phillipsite. When calcium hydroxide is generated during the hydration of cement, the SiO_2 and Al_2O_3 content of natural zeolites reacts with it to create C-S-H (Calcium-Silicate-Hydrate) gels and aluminates (Akgun Yasemin. 2019). The matrix is more compact in M6 than M3, possibly because of the smaller amount of CH in LC^3 that can react with the constituents of the soil-quarry dust mixture. LC^3 cements have decreased early strength due to a diluting effect of limestone and their limited pozzolanic reactivity during early ages, these reactions form C-S-H which is the binding gel for the matrix. Overall, both OPC and LC^3 addition improved microstructural characteristics, resulting in the formation of a more stable and dense soil structure. The formation of a matrix in M3 indicates that LC^3 is a viable sustainable alternative, however, the matrix is more compact in the OPC sample, suggesting that LC^3's stabilizing power is less efficient as was observed in the preliminary analysis.

The rapid dehydration of LC^3 was observed in the DTG graph due to a strong decomposition peak of C-A-S-H. The DTG graph however shows a low amount of hemicarboaluminate as they form

at later stages. This could also be the reason for a less compact LC^3 matrix as observed by the SEM which would result in a lower strength of the cement. The preliminary results however indicate a comparable increase in strength for both OPC and LC3 after 14 days of curing (Fig. 26).

The loss of moisture from the soil is the cause of shrinkage in the volume analysis. As shown by the XRD, the samples contain a large amount of kaolinite. The higher particle size of kaolin clay implies that most soil water is not tightly adsorbed to the surface and can hence evaporate easily leading to a shrinkage from water loss. Rotana H et al (2022) also found that the improved microstructure of LC^3 mixtures explain their higher shrinkage relative to OPC counterparts. A preventative measure to reduce shrinkage is to limit the plasticity (and thus water affinity). In the preliminary analysis, the addition of 5% of both LC^3 and OPC reduced the plasticity index and hence shrinkage and increased its load bearing capacity. The proctor test also showed an increase in density and reduction in moisture content due to an increase in compaction of the soil particles at a 5% cement dosage. These effects could also be attributed to a denser matrix as shown by the SEM. It can thus be inferred that LC^3 is a viable alternative to OPC as they both exhibit minimal shrinkage. However, LC^3 exhibits more shrinkage in comparison to OPC which also indicates its lower efficiency.

The OPC calorimetry plot shows a higher exothermic peak as compared to LC^3 which indicates slower reaction kinetics in the LC^3 sample. The cumulative heat plot also indicates a rapid early hydration in OPC due to a higher heat release in comparison with LC^3. The hydration reactions were also investigated using the SEM and XRD which indicate a lower amount of hydration products in the LC^3 sample. A possible reason for reduced clinker hydration in LC^3 could be a decrease in pore solution pH. Avet F et al (2019) also found that incorporating Al into C-S-H gel enhances alkali binding which results in a decrease in the pH of the pore solution, inhibiting the hydration of clinker phases.

CHAPTER 8 - CONCLUSION

This study showed a comprehensive study aimed at assessing the suitability of limestone calcined clay cement as a sustainable alternative to ordinary Portland cement in soil stabilization at a macro and micro scale. Based on the results, the following conclusions can be drawn:

- According to XRD data, the soil had a kaolinite content of 85.8%. Kaolinite is classified as a non-expansive clay, however, the one used in this study was found to be a plastic kaolin as expansion and shrinkage occurred due to absorption and desorption of water. Aluminous zeolites such as phillipsite and analcime were found in the quarry dust. These zeolites were shown to have positive properties such as high pozzolanic activity, high silica alumina content and low heat of hydration which could increase their usage capacities in soil stabilization. Though in low amount due to the low cement ratio, the XRD showed the formation of hydration products in both the LC^3 and OPC samples.
- The SEM showed a compact matrix for both LC^3 and OPC cement mixtures indicating that stabilization had occurred which proves LC^3 to be a suitable sustainable alternative to OPC. The matrix was however more compact in OPC than LC^3 which shows a higher stabilization power in OPC.
- The mass loss in the TGA analysis of the soil-LC^3 mixtures is mainly due to dehydration and dihydroxylation of clay and the dehydration of the zeolites analcime and phillipsite.
- LC^3 exhibits a higher volume strain to OPC due to its lower stabilization power.
- In comparison to LC^3, OPC showed a higher exothermic peak in the calorimetry analysis which indicates slower reaction kinetics in LC^3.

The results of this study promote LC^3 as a sustainable alternative to OPC in the stabilization of expansive soils. In summary LC^3 exhibits a comparable performance to its reference (OPC) at a macro and micro scale though in general OPC displayed an overall better stabilizing power.

The current and future urbanization trends and population increase will require an increase in the amount of construction and hence the widespread utilization of OPC in construction which would not only depletes natural resources but also cause a huge environmental impact in terms of carbon emission. Therefore, a compromise between sustainability and cement performance will have to be taken. Further studies can be done on the calcination technology of LC^3 to increase its performance. Despite the relative maturity of research on calcination technology, further studies can be done to critically analyze and characterize the clay available to design appropriate extraction, pre-processing, calcination, and cooling processes that would influence the clay's maximum reactivity and thus increase its performance.

LIST OF FIGURES

LIST OF TABLES

REFERENCES

Adaska W S and Luhr R D. “Control of reflective cracking in cement stabilized pavements”. *Control of Reflective Cracking in Cement Stabilized Pavements,* 5th International RILEM Conference, Limoges, France, May (2004).

Bish, D.L.; Post, J.E. 1993. “Quantitative mineralogical analysis using the Rietveld full-pattern fitting method”. *American Mineralogist,* Vol. 78, p. 932-940.

Meyer, J.H. (2013) The soil and its environment, in *Good Management Practices Manual for the Cane Sugar Industry* (eds J.H. Meyer, P. Rein, P. Turner, K. Mathias and C. McGregor), International Finance Corporation, Sao Paulo, Brazil.

Ahmed Z. Khalifaa, Özlem Cizera, Yiannis Pontikesb, Andrew Heathc, Pascaline Patureaud, Susan A. Bernale, Alastair T.M. Marsh. “Advances in alkali-activation of clay minerals”. *Cement and Concrete Research,* Volume 132, June 2020, 106050

Akgun Yasemin. “A Comparative Study: Blended Cements Containing Analcime and Clinoptilolite”. *Journal of Natural and Applied Sciences* Volume 23, Issue 3, 748-758, 201.

Ali MS, Khan I A, Hossain I M. “Chemical analysis of ordinary Portland cement of Bangladesh” *Chemical Engineering Research Bulletin* 12 (2008) 7 -10.

Rietveld H M. “A profile refinement method for nuclear magnetiic structures”. *J. Appl. Cryst.* (1969). 2, 65.

O'Flaherty, C. A.; David, H. T.; and Davidson, D. T. (1961) "Relationship Between the California Bearing Ratio and the Unconfined Compressive Strength of Sand-Cement Mixtures," *Proceedings of the Iowa Academy of Science, 68(1),* 341-356.

Andrei A. Bunachiu, Elena Gabriela Udristoiu¸ and Hassan Y. Aboul-Enein. “X-Ray Diffraction: Instrumentation and Applications”. *Critical Reviews in Analytical Chemistry* (2015) 45, 289–299.

Avet F, Scrivener K. “Investigation of the calcined kaolinite content on the hydration of Limestone Calcined Clay Cement (LC3)”. *Cement and Concrete Research* (2018) 107: 124-135.

B.V. Bahoria, D.K. Parbat and P.B. Nagarnaik, Characterization Study of Natural Sand, Quarry Dust, Waste Plastic (LDPE) to be used as a Fine Aggregate in Concrete. *International Journal of Civil Engineering and Technology*, 8(3), 2017, pp. 391–401

Padmanabhan, Eswaran & Reich, Paul. (2022). “World soil map based on soil taxonomy”. *Reference Module in Earth Systems and Environmental Sciences* 10.1016/B978-0-12-822974-3.00118-X.

Barman, D and Dash, S.K. “Stabilization of expansive soils using chemical additives: a review”. *J. Rock Mech. Geotech. Eng*. 14 (4), 1319–1342 (2022).

Belay Z Dilnesa. “Application of thermogravimetric method in cement science” *EMPA Materials Science and Technology*.

British Standards; BS 812: Part 101, Part 103-1, Part 105, Part 110 and Part 111; *Structural use of concrete.*

Chenarboni, H.A, Lajevardi, S.H, MolaAbasi, H, Zeighami, E 2. “The effect of zeolite and cement stabilization on the mechanical behavior of expansive soils”. *Construction and Building Materials* 272, 121630 (2021).

Christidis E G. “Advances in the characterization of industrial materials”. *European Mineralogical Union and the Mineralogical Society of Great Britain and Ireland, London* (2011)

Chung, Chul-Woo Kim, Ji-Hyun Lee, Soo-Yong. “The Use of Semi-Adiabatic Calorimetry for Hydration Studies of Cement Paste”. *J. Korea Inst. Build. Constr.* Vol. 16, No. 2 : 185-192 / Apr, (2016).

D. Rykl and F. Pechar. “Thermal decomposition of natural phillipsite”. Zeolite Vol. 11 September/October (1991)

Daniela Novembre and Domingo Gimeno. “Synthesis and characterization of analcime (ANA) zeolite using a kaolinitic rock”. *Nature Scientific Reports* (2021) 11:13373

Di Dai, Jie Peng, Renjie Wei, Liangliang Li, Hongmin Lin. “Improvement in dynamic behaviors of cement-stabilized soil by super-absorbent-polymer under cyclic loading”. Soil Dynamics and Earthquakes Engineering 163 (2022) 107554

Elizaveta Ermilova, Zagira Kamalova, Rakhimov Ravil. “Influence of clay mineral composition on properties of blended portland cement with complex additives of clays and carbonates”. *IOP Conf. Series: Materials Science and Engineering* 890 (2020) 012087

Fernandez, R., Martirena, F., Scrivener, K.L., 2011. “The origin of the pozzolanic activity of calcined clay minerals: a comparison between kaolinite, illite and montmorillonite”. *Cement and concrete*, res. 41, 113–122 (2011).

Ferreira E J and Gardolinski C. “ Interlayer grafting and delamination of Kaolinite”. Christian-Albrechts-University in Kiel, Germany (2005)

G. Habert a,*, J.B. d'Espinose de Lacaillerie b , N. Roussel. "An environmental evaluation of geopolymer based concrete production: reviewing current research trends" *Journal of Cleaneer Production* 19 (2011) 1229-1238

Halsted, G.E., W. S. Adaska, and W. T. McConnell. "Guide to Cement-Modified Soil (CMS)". *Portland Cement Association, Skokie,* IL. http://secement.org/wp-content/uploads/2017/04/EB242.pdf. (2008)

Jasmund K. and Lagaly G. "Tonminerale und Tone: Struktur." Eigenschaften und Einsatz in Industrie und Umwelt, Steinkopff, Darmstadt, Germany (1993).

Kaolins, Bentonites, Palygorskitesepiolite, and Common Clays". *Developments in Clay*

Karen Scrivenera, Fernando Martirena, Shashank Bishnoic, Soumen Maityd "Calcined clay limestone cements (LC3)" *Cement and Concrete Research* 114 (2018) 49-56

Kisunge J. "Road Construction Materials, Basic Knowledge and Test Procedure" (2012)

L. A. Silva1, B. O. Nahime 1 , E. C. Lima , J. L. Akasaki, I. C. Reis. "XRD investigation of cement pastes incorporating concrete floor polishing waste" *Cerâmica* 66 (2020) 373-378

Maria Luiza P.M. Gomes, Elaine A.S. Carvalho, Larissa N. Sobrinho, Sergio N. Monteiro, Rubén J.S. Rodriguez, Carlos Maurício F. Vieira "Production and characterization of a novel artificial stone using brick residue and quarry dust in epoxy matrix". *J Materres technology*. 2018;7(4):492–498.

Meenakshi Sharma, Shashank Bishnoi, Fernando Martirena, Karen Scrivener "Limestone calcined clay cement and concrete: A state-of-the-art review" Cement and Concrete Research 149 (2021) 106564

Mo Zhang, Hong Guo, Tahar El-Korchi, Guoping Zhang, Mingjiang Tao. "Experimental feasibility study of geopolymer as the next-generation soil stabilizer" *Construction and Building Materials* 47 (2013) 1468-1478

Soil Survey Staff. 1975. :Soil Taxonomy: A basic system of soil classification for making and interpreting soil surveys". *USDA-SCS Agric. Handbook*. 436, U.S. Government Printing Office, Washington, DC.

Murray H. :Applied Clay Mineralogy: Occurrences, Processing and Applications of

Nauman Ijaz, Weimin, Zia ur Rehman, Zain Ijaz.“Novel application of low carbon limestone calcined clay cement (LC3) in expansive soil stabilization: An eco-efficient approach’’. *Journal of Cleaner Production* 371 (2022) 133492.

Ng, H.M. & Mohamad saidi, Norshahirah & Omar, Fatin Saiha & Kasi, Rameshkasi & T subramaniam, Ramesh & Baig, Shahid. “Thermogravimetric Analysis of Polymers”. 1-29. 10.1002/0471440264.pst667 (2018).

Obrist D M, Kannan R, Schmidt J T , Kober T. “Decarbonization pathways of the Swiss cement industry towards net zero emissions”. *Journal of Cleaner Production* 288 (2021) 125413.

Okiemute Roland Ogirigbo. “Influence of Slag Composition and Temperature on the Hydration and Performance of Slag Blends in Chloride Environments” https://www.researchgate.net/publication/305641458

Onyelowe Ken , Okafor F. O. and Nwachukwu D. G. “Geophysical use of quarry dust(Aa Admixture) as applied to soil stabilization and modification- A review”. *ARPN Journal of Earth Sciences* VOL. 1, NO. 1, OCTOBER 2012.

P. Narasimha Reddy, J. Ahmed Naqash. “Experimental Study on TGA, XRD and SEM Analysis of Concrete with Ultra-fine Slag”. *IJE TRANSACTIONS B: Applications Vol.* 32, No. 5, (May 2019) 679-684.

Paul E. Stutzman, Pan Feng, and Jeffrey W. Bullard. “Phase Analysis of Portland Cement by Combined Quantitative X-Ray Powder Diffraction and Scanning Electron Microscopy” *Journal of Research of the National Institute of Standards and Technology Volume* 121 (2016).

Rebecca A. Sanderson, Gavin M. Cann & John L. Provis. “Comparison of calorimetric methods for the assessment of slag cement hydration”. *Advances in applied ceramics*, 2017 VOL. 116, NO. 4, 186–192.

Refiloe Mokoena, Tshepo Motau and Georges Mturi. “Investigating the use of isothermal calorimetry for predicting physical properties of cements”. *Ycrets Technical Paper* 1 September (2022)

Richards A. Rowland. “Differential thermal analysis of clays and carbonates”. C*lays and Clay Minerals,* 1(1), 151–163, 1952.

Rotana Hay, Liang Li, Kemal Celik. “Shrinkage, hydration, and strength development of limestone calcined clay cement (LC3) with different sulfation levels”. *Cement and Concrete Composites* 127 (2022) 104403

Ruben Snellings, Gilles Mertens and Jan Elsen "Supplementary Cementitious Materials" *Reviews in Mineralogy & Geochemistry* Vol. 74 pp. 211-278, 2012

Run-Sheng Lin, Yi Han, Xiao-Yong Wang. "Macro–meso–micro experimental studies of calcined clay limestone cement (LC3) paste subjected to elevated temperature". *Cement and Concrete Composites* 116 (2021) 103871.

Science, vol. 2. Elsevier, Amsterdam, 188 pp (2007)

Sridharan A, Soosan T G, Babu T J, Abraham B M. "Shear strength studies on soil quarry dust mixtures". *Geotechnical and Geological Engineering* 24: 1163-1179 (2006).

Suraj D. Khadka, Priyantha W. Jayawickrama, Sanjaya Senadheera, Branimir Segvic. "Stabilization of highly expansive soils containing sulfate using metakaolin and fly ash based geopolymer modified with lime and gypsum''. *Transportation* Geotechnics 23 (2020) 100327.

Susan A. Bernal, Maria C. G. Juenger, Xinyuan Ke, Winnie Matthes, Barbara Lothenbach, Nele De Belie , John L. Provis. "Characterization of supplementary cementitious materials by thermal analysis". *Materials and Structures* (2017) 50:26

Swapnil Namdev Sutar, Prajyot Vitthal Patil, Rohit Vitthal Chavan, Mayur M. Mask. "Study and Review of Ordinary Portland Cement" *ASEAN Journal of Science and Engineering* 1(3) (2021) 153-160.

Stan CV, Beavers CM, Kunz M, Tamura N. "X-Ray Diffraction under Extreme Conditions at the Advanced Light Source". *Quantum Beam Science*. 2018; 2(1):4.

Wypych F and Freitas A R. "Clay minerals- Classification structure and properties"*Developments in Clay Science*, Volume 10, Pages 3-35 (2022)

Young J F. Portland Cement. *Encyclopedia of Materials: Science and Technology* ISBN: 0-08-0431526 pp. 7768–777 (2001).

Yu Xiao, Liyuan Tong, Hongbo Che, Qiwen Guo, Huangsong Pan. "Experimental studies on compressive and tensile strength of cement-stabilized soil reinforced with rice husks and polypropylene fibers" Construction and Building Materials 344 (2022) 128242.

Yubin Cao, Yanru Wang, Zuhua Zhang, Yuwei Ma d , Hao Wang. "Thermal stability of limestone calcined clay cement (LC3) at moderate temperatures 100–400 ◦C". *Cement and Concrete Composites* 135(2023) 104832.

Yubin Cao, Yanru Wang, Zuhua Zhang, Yuwei Ma,Hao Wang. “Recent progress of utilization of activated kaolinitic clay in cementitious construction materials” *Composites Part B* 211 (2021) 108636.

Zaefferer S. “Scanning electron microscopy and electron backscatter diffraction”. *European Mineralogical Union Notes in Mineralogy* 16:37-95 (2017)